

## ACKNOWLEDGMENTS

The authors are deeply indebted to Professor B. L. Cohen for permitting them to use the University of Pittsburgh cyclotron for taking the data reported in this work. Thanks are also due to Professor R. M. Drisko for his help in doing the DWBA calculations. The authors are grateful to Professor J. D. Fox for a thorough review of the final manuscript. They sincerely appreciate the support and encouragement of Professor

R. H. Davis. The authors feel particularly indebted to Mrs. Meyers and collaborators for a very careful scanning of the nuclear-emulsion plates. The patient help of the secretarial staff of the Tandem Van de Graaff Accelerator Program is sincerely appreciated. Some of the DWBA calculations used in the present work were performed at the computing center of the University of Pittsburgh, which is partially supported by the National Science Foundation (Grant No. G-11309).

## New Type of Accelerator for Heavy Ions\*

G. S. JANES, R. H. LEVY, H. A. BETHE,† AND B. T. FELD‡

*Avco-Everett Research Laboratory, Everett, Massachusetts*

(Received 10 December 1965)

A new device, called the heavy ion plasma accelerator (HIPAC), which may be capable of accelerating ions of any atomic number to energies sufficient to overcome the nuclear Coulomb barrier, is described. A closed potential well is created by filling a toroidal vacuum chamber with electrons; the electrons are contained by a magnetic field whose intensity is so low that its effect on the ions can be neglected. Ions are both accelerated and trapped in the well; the trapping effect allows sufficient time for the ions to become highly stripped by electron impact. The very large ion energies that can be achieved in this way would allow a wide variety of nuclear reactions to be studied, including inverse fission. The present primitive state of development of the HIPAC is described, and the future prospects assessed.

## I. INTRODUCTION

A NEW device, called the heavy ion plasma accelerator (HIPAC), is suggested which may make possible the performance of presently unattainable experiments involving nuclear and energetic atomic reactions between heavy ions. Based on small scale experiments<sup>1,2</sup> and theoretical<sup>3,4</sup> work already performed, the outlook for the ultimate construction of the HIPAC is favorable, but there are nevertheless important unanswered questions having to do with the attainment of useful operating conditions.

In outline, the HIPAC utilizes the potential well due to a cloud of electrons; the electron cloud is established and controlled through the use of time-varying magnetic fields. The potential well serves the dual function of accelerating and trapping heavy ions that may be introduced, while the electrons of the cloud produce a

high degree of stripping of these ions. Since the ion energy is proportional to the charge state as well as to the well depth, a well depth of 20 million volts would create center-of-mass energies sufficient to overcome the Coulomb barrier for collisions between nuclei of all species (see Fig. 1). For the heavy elements ( $Z \geq 20$ ) this condition cannot be matched by any presently existing or proposed device. Well depths such as this, while representing an extrapolation on present achievements, appear nevertheless to be accessible in apparatus of relatively modest dimensions and cost. If they can indeed be reached, a considerable range of experiments involving nuclear reactions between heavy elements becomes accessible. Thus, for example, collisions between like or unlike nuclei of atomic number in the medium range 30-50 should give rise to the inverse of the nuclear-fission process. Studies of inverse fission could cast important new light on the dynamics of the fission process. While available "heavy" ion accelerators have already uncovered an interesting variety of new interactions, they have only scratched the surface of the possibilities which should be available to the HIPAC for which there are no inherent limitations on the nuclei available for study. Reactions between complex nuclei are presently achieved<sup>5</sup> by accelerating projectiles in a

\* This work has been supported by the U. S. Air Force Office of Scientific Research of the Office of Aerospace Research, U. S. Air Force under Contract No. AF49(638)-1553.

† Permanent address: Cornell University, Ithaca, New York.

‡ Permanent address: Massachusetts Institute of Technology, Cambridge, Massachusetts.

<sup>1</sup> G. S. Janes, *Phys. Rev. Letters* **15**, 135 (1965).

<sup>2</sup> G. S. Janes, R. H. Levy, and G. E. Cooper, *Bull. Am. Phys. Soc. II* (1966) (to be published).

<sup>3</sup> R. H. Levy, *Phys. Fluids* **8**, 1288 (1965).

<sup>4</sup> O. Buneman, R. H. Levy, and L. M. Linson, *J. Appl. Phys.* (to be published).

<sup>5</sup> E. L. Hubbard, *Ann. Rev. Nucl. Sci.* **11**, 419 (1961).

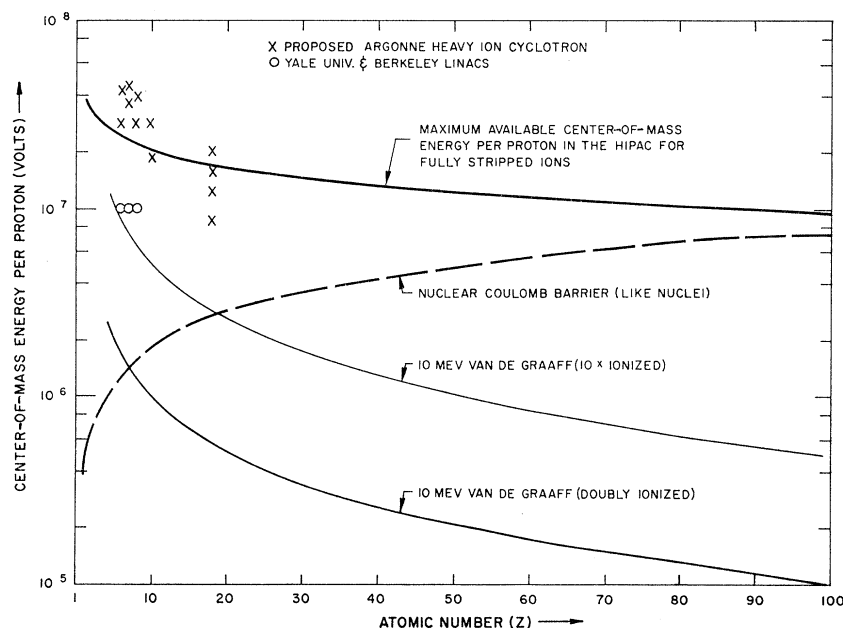


FIG. 1. The potentialities of the HIPAC for producing nuclear reactions between heavy ions are illustrated in this figure. The heavy line indicates the center-of-mass energies available (per proton) for collisions between like nuclei in the HIPAC whose parameters are discussed in detail in this paper. The ions are not assumed to be completely stripped since it is not necessary to accomplish complete stripping in order to achieve the desired ion energies. Although the well depth of the HIPAC is assumed to be 20 million volts, a stripped ion will be oscillating through the full well depth only if all the ionizations take place near the top of the well, i.e., near the wall. An allowance for the nonfulfillment of this condition, based on the calculation of Appendix A, has been made. After 30 ionizations, the effective well depth is reduced to about 7 million volts. For comparison, the Coulomb barrier energy (per proton) for collisions between like nuclei is shown (dashed line). Also plotted is the energy available in the center-of-mass frame from a 10-million-volt Van de Graaff operating with 2- and 10-times ionized ions, and the energies available from some existing (Ref. 5) and proposed (Ref. 6) heavy-ion accelerators; these energies are also calculated on the basis of collisions between like nuclei.

linear accelerator or a cyclotron, and directing the accelerated beam onto a target. Since appreciable currents of ions more than about six (or at the most eight)<sup>6</sup> times ionized are not presently available, practical limits on accelerator size have restricted the projectiles to the elements lighter than neon (or, in some cases, argon). As a result, among all the possible nuclear reactions between stable isotopes, only a small fraction are presently attainable. Essentially all the remaining nuclear reactions between pairs of elements heavier than neon should be accessible to the HIPAC.

Many of the reactions believed to be important in the genesis (cooking) of the elements in cosmological processes<sup>7,8</sup> could be studied in the HIPAC, since the ionic component of our plasma will have velocities corresponding to temperatures in excess of  $10^{10}$  °K. Collisions between intermediate atomic weight nuclei should lead to product nuclei on the neutron-poor side of the nuclear stability curve, relatively far from the nuclear stability line. This region is inaccessible to reactors and goes considerably beyond that generally

accessible to cyclotrons. Aside from studies of the radioactive decay properties of such nuclei, it is possible that new radioactive species may become available in appreciable quantities which may be utilizable in other fields as well.

The HIPAC may also have useful application in the field of atomic physics, particularly in the field of stellar spectroscopy. For this is, after all, a device for producing highly ionized atoms, and the atomic radiations from such atoms could be studied as well. So, in effect, it should be possible to study the spectra of elements in highly ionized conditions much more closely approximating stellar circumstances than are now available in terrestrial laboratories.

The HIPAC, as presently envisaged, would consist of an evacuated toroidal conducting chamber. The interior of the chamber is filled with electrons which have the effect (shown in Fig. 2) of depressing the electrostatic potential of the circular axis relative to the potential of the containing vessel. The potential well thus formed is "closed" in the sense that the "bottom" is not in contact with any material surfaces. An ion formed just inside the wall of the vessel would be accelerated toward the bottom of the well (i.e., the circular axis). On reaching this axis the ion will have acquired an energy proportional to the voltage drop and to its charge state. At this point in a conventional

<sup>6</sup> J. J. Livingood, T. K. Khoe, W. J. Ramler, K. W. Johnson, G. S. Mavrogenes, and R. A. Winje, *IEEE Trans. Nucl. Sci.* **NS-12**, 484 (1965).

<sup>7</sup> E. M. Burbidge, G. R. Burbidge, W. A. Fowler, and F. Hoyle, *Rev. Mod. Phys.* **29**, 457 (1957).

<sup>8</sup> W. A. Fowler and J. Vogl, *Lectures in Theoretical Physics* (University of Colorado Press, Boulder, Colorado, 1964), Vol. VI.

high-voltage machine, the ion would strike the cathode, and its useful life would be over. In the HIPAC, however, the "cathode" consists only of the electron cloud filling the device. The ion therefore continues straight on, "climbing" the other side of the potential well, until it comes to rest short of the wall at the potential at which it was released. At this point it turns around, and recrosses the well, the process continuing until terminated by a collision or some other event. The essential point is that ions are trapped in the acceleration region. If we now introduce more ions, the possibility will exist of collisions between them in the vicinity of the circular axis, where both ions are highly energetic. We thus have a "clashing beam" machine, except that the ions can approach the bottom of the well from essentially any direction. It is therefore more appropriate to describe the ion cloud as having a temperature; in interesting cases involving stripped heavy ions this temperature can be many hundreds of millions of electron volts.

There are three important questions to ask concerning the electron cloud:

- (a) How is it to be maintained in position?
- (b) How is it to be placed in position initially?
- (c) Are there any serious instabilities or other losses?

The importance of question (a) lies in the observation that the same gradient of the electrostatic potential which accelerates and traps the ions tends to drive the electrons to the wall of the HIPAC. The key to containing the electrons is the introduction of a magnetic field parallel to the circular axis of the device. This field may be due to windings around the toroidal vacuum vessel. Now in the presence of crossed magnetic and electric fields charged particles of either sign tend to drift in the direction perpendicular to both fields with speed  $E/B$  (Fig. 3). In our case this yields periodic circular orbits *around* the circular axis (Fig. 4). The magnetic field therefore changes the electron trajectories from a very short one-way trip to the wall into a circular motion which would in principle last indefinitely.<sup>9</sup>

With respect to question (b), it is proposed to use a method called "inductive charge injection" to establish the electron cloud in its place. This method involves placing electrons on magnetic-field lines and then compressing the magnetic field. Since this compression can be thought of in terms of carrying magnetic-field lines away from the wall towards the bottom of the potential well, and since individual electrons will tend to stay on individual magnetic field lines during the compression process, the whole arrangement conceptually resembles a Van de Graaff generator in which the material moving belt has been replaced by a belt of

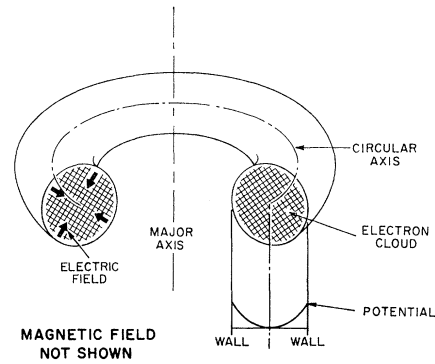


FIG. 2. This figure shows the electrostatic configuration of the heavy ion plasma accelerator, or HIPAC, and the associated closed potential well. The way in which a magnetic field is used to keep the electron cloud in position is not shown here, but is illustrated in Fig. 4.

moving magnetic-field lines. Inductive charge injection has been successfully tested in a small-scale experiment.<sup>2</sup>

Since the "belt" is only moving "forwards" when the magnetic-field strength is increasing, it is essential that any instability or other loss mechanism which allows the electrons to slip back toward the wall be slow compared to the time scale on which the "belt" can be moved forward. This time is, of course, the time for energizing the magnetic field and will typically be 20–100  $\mu\text{sec}$ . Any loss slower than this will have no effect other than limiting the time for which the potential remains high. With electron clouds, however, the characteristic frequencies (plasma frequency, cyclotron frequency) are large compared with the frequencies implied by the rise times for the magnetic field mentioned above. The possible existence of serious instabilities must therefore be suspected. For the

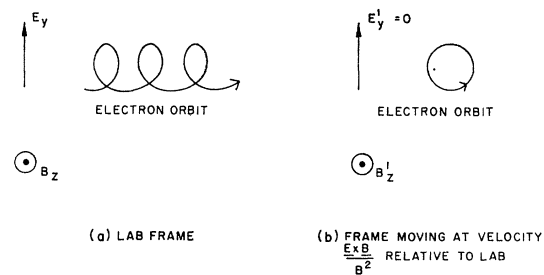


FIG. 3. In crossed electric and magnetic fields [Fig. 3(a)], a charged particle follows a cycloidal path. This motion can be resolved [Fig. 3(b)] by transforming to a frame moving at velocity  $(\mathbf{E} \times \mathbf{B})/B^2$  relative to the laboratory. In this frame the electric field  $E'_y$  vanishes, leaving the particle to make Larmor circles around the magnetic field lines. The cycloidal motion in the lab frame therefore consists of a uniform drift perpendicular to  $\mathbf{E}$  and  $\mathbf{B}$  with speed  $E/B$ , and a circular motion around the field lines. These pictures are valid provided only that  $E/B < c$ . If this condition is not met, i.e., if  $E/B > c$ , the transformation to the frame of Fig. 3(b) is not allowed. In this case the particle can be indefinitely accelerated by the electric field. Note that the  $E/B$  drift is independent of the charge or mass of the particle; these quantities affect only the size (and sense) of the Larmor circle shown in Fig. 3(b). The sense shown corresponds, as indicated, to an electron.

<sup>9</sup> Earnshaw's theorem demonstrates the impossibility of static equilibrium for a collection of free charges; in the HIPAC we are dealing with a dynamic equilibrium beyond the scope of Earnshaw's theorem. A well-known example of this situation is to be found in the solar system which is clearly in dynamic but not in static equilibrium.

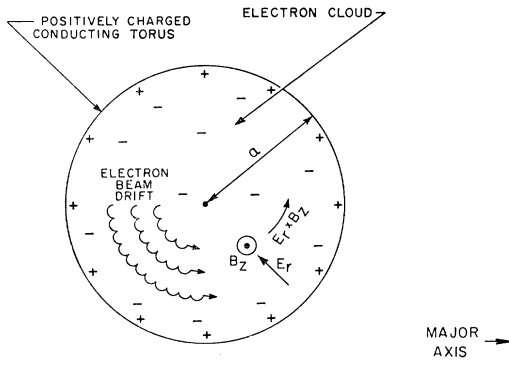


FIG. 4. Electron containment by a magnetic field in the HIPAC. The size of the small orbits is a measure of the electron "temperature." For the large (drift) orbit, the electric and magnetic forces are nearly in balance: the centrifugal force (on an electron) is less than either by the factor  $q = n_e m_e / \epsilon_0 B^2 \ll 1$ . In a torus the intensity of the magnetic field decreases with distance from the major axis. The effect of this is to shift the whole electron orbit slightly sideways, but it remains cyclic. The electric field in the HIPAC is entirely due to the space charge of the electrons; this yields essentially a solid-body rotation about the circular axis of the torus for the electron cloud.

moment we shall merely note that the basic instabilities of electron clouds of the type required are fairly well known, and that, with appropriate selection of parameters, a considerable and adequate degree of stability has been observed in small-scale experiments,<sup>1</sup> and can be explained theoretically.<sup>3,4</sup> This point is discussed at length in the following sections, together with more thorough explanations of the equilibrium of the HIPAC, and of the method of inductive charge injection.

Although the motions of the electrons can be understood in terms of the crossed-field drift, and although this drift is the same for all particles independent of charge, sign or mass, the ion motions in the HIPAC cannot be explained on this basis. The reason for this seeming paradox is that, although the ions would "like" to drift at the  $E/B$  velocity, there will in general be insufficient room to accomplish the necessary acceleration. More formally, the ion Larmor radius at the  $E/B$  velocity is likely to be many times larger than the size of the HIPAC; the effect of this situation on the ion trajectories is illustrated in Fig. 5. Note the minor importance of the magnetic field: the ions are essentially oscillating backwards and forwards across a closed potential well.

If an ion in the condition typified by Fig. 5 undergoes further ionization, two things will occur simultaneously: The electric force on the ion is increased resulting in a greater ion energy when at the bottom of the potential well, and the magnetic force is increased, resulting in a greater curvature of the ion trajectory. There is a critical condition when the Larmor radius of the ion just equals the radius of the HIPAC. At this point, the ion velocity produced by falling through the full depth of the well is close to the  $E/B$  velocity. In a sense, this is an ideal operating condition for the HIPAC, for any

further ionization will produce a Larmor radius smaller than the radius of the HIPAC; in this condition the ion is prevented by the magnetic field from falling through the full depth of the potential well, but will tend instead to acquire a motion resembling that of the electrons illustrated in Fig. 4, that is, at the  $E/B$  velocity.

The essential point is this: the HIPAC is a crossed-field machine, and tries to bring all charged particles up to the  $E/B$  velocity. This can be accomplished only if there is enough room. Plenty of room is available for the acceleration of the electrons, but not for the ions, at least when they are only slightly stripped. The ideal condition for the ions would be to have a Larmor radius close to the radius of the HIPAC when at the velocity corresponding to the full depth of the potential well, but, as we shall see, interesting ion energies can be attained long before this condition is reached. By way of example, if  $E/B = 0.26c$ , the energy associated with the electron drift is only 18 keV, whereas an ion at this speed has an energy  $33A$  MeV. While 33 MeV is not an especially interesting proton energy, the corresponding figures for heavy ions are highly attractive.  $33A$  MeV is in all cases far above the Coulomb barrier energy for nuclear collisions which is on the order of  $3A$  MeV for the heaviest ions. If the depth of the well is 20 million volts, a fully stripped heavy ion can acquire up to  $8A$  MeV, and even this figure is well above the Coulomb barrier. At this energy, the ion speed is well under the figure of  $0.26c$  quoted above and it follows that the effect of the magnetic field on the ion is slight.

The various numbers that have been quoted all refer to a sample HIPAC of minor radius 20 cm, major radius 1 m, and well depth 20 million volts. This particular HIPAC is discussed in detail in this paper. Figure 6 is a "map" of the region of parameter space which should be accessible to this HIPAC. While the various features of this map are discussed later in this paper, we can note here that the hatched region is presently thought to be available for exploitation. Thus, as the magnetic-field strength increases from 1 to 30 kG, the

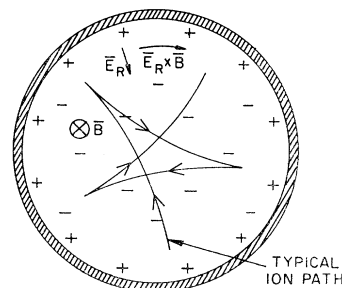


FIG. 5. This figure illustrates a typical ion path in the HIPAC under conditions for which the ion Larmor radius at the energy associated with the depth of the potential well is several times larger than the minor radius of the HIPAC. Note the crossings of the path at all angles in the low-potential central region of the HIPAC.

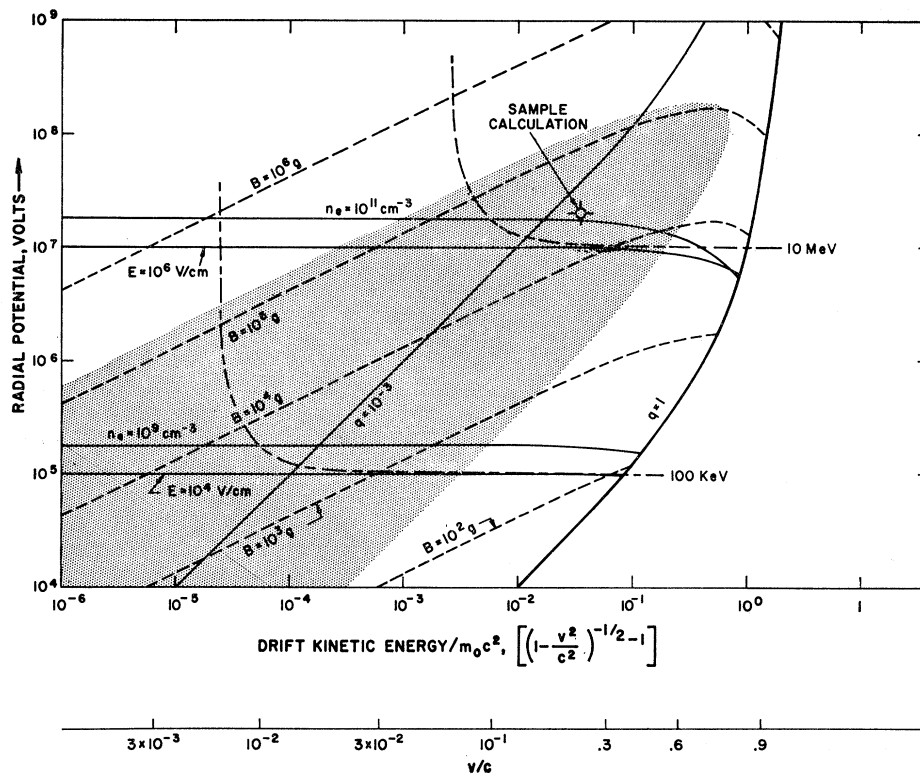


FIG. 6. This is a "map" of the region of parameter space accessible to a HIPAC having a 20-cm minor radius. Absolute radial voltage is plotted against drift kinetic energy, that is, the energy associated with motion at the drift speed  $E/B$ . Lines of constant electric field (at the wall), magnetic field and electron number density are shown.  $q$  is the nondimensional ratio  $\omega_p^2/\omega_c^2$  ( $\omega_p$  is the electron plasma frequency,  $\omega_c$  the electron cyclotron frequency). The HIPAC is thought to be stable for  $q \leq 0.03$ . Points within the hatched area are presently believed to be accessible. This area is limited by the stability condition mentioned, and by the practical limit on magnetic field intensities. The lines marked "100 keV" and "10 MeV" represent the energies achieved by a proton released from rest at the wall. These energies can never exceed the energy corresponding to the  $E/B$  velocity, but will be less if there is insufficient room to accelerate the particle to this velocity. The "Sample Point" represents the HIPAC for which the parameters are given in detail in Sec. II-4, and which forms the basis of the proposed experimental program. A map similar to this but for a 10-cm minor radius HIPAC is shown in Fig. 25; on this map are marked the parameters of experiments already performed, even though these were not in toroidal geometries. A 1-m map is shown in Fig. 26. Further details of the calculations going into these maps are given in Sec. II.

available potentials should increase from over  $10^5$  V to about  $3 \times 10^7$  V. The sample calculation is at  $B = 26$  kG. A similar map for a 10-cm HIPAC is shown in Fig. 25 and on this map the experiments already performed are indicated.

In addition to the energy associated with the drift motion (18 keV in the example quoted), the electrons will possess an energy associated with their Larmor orbiting as viewed in a frame moving at the drift velocity. This energy, which can loosely be called "thermal," may be larger than the drift energy, especially for electrons near the circular axis of the HIPAC which have undergone a large magnetic compression in the inductive charging process. Both of these energies are large enough to permit the electrons to produce by impact the high degree of stripping of the ions necessary if the latter are to acquire the desired high energies. Since the ions are trapped in the potential well, there will generally be sufficient time available to accomplish this stripping; this situation is in striking contrast to the situation in typical ion sources

from which the available currents become negligible after at most 6 or 8 ionizations. The critical point is that for heavy ions, stripping, trapping, and acceleration all take place in the same region of space.

A vital feature of the HIPAC is that it uses the properties of clouds of electrons in crossed electric and magnetic fields. A large body of knowledge already exists concerning the behavior of such clouds, especially as applied to other devices that use crossed-field electron beams. The most important of these devices are the crossed-field microwave magnetron, the Phillips ionization gauge, and related microwave and vacuum devices. These devices, and their underlying theory, are briefly discussed in the next sections; here we note that crossed-field electron beam are rather well understood, and experiments relating to them are essentially in good agreement with theoretical treatments. They are on the whole "well behaved," especially when compared with neutral plasmas.

Since the HIPAC makes use of the collective properties of a cloud of free charged particles in a magnetic

field, the use of the term "plasma" in describing it seems justified, even though the cloud consists principally of charged particles of one sign (electrons) and is therefore far from electrically neutral as a whole. We have seen how it can be used to accelerate ions, and it is from this consideration that we apply the name "plasma accelerator," to the device. A different view of the acceleration process is as follows: an ion released at the wall falls into the bottom of the potential well, gaining kinetic energy. When it is there, its positive charge reduces somewhat the depth of the well it is in, and therefore reduces somewhat the potential energy of every electron in the device. Thus, a tiny fraction of the energy of each electron in the machine has been converted into the kinetic energy of a single ion. For a device acting in this manner, the name "plasma accelerator" seems very suitable.

Although the heavy ion reactor appears the most immediately promising application of the HIPAC, two other ideas appear interesting and worthy of study, but are definitely further off in time. We mention these ideas here, as they are of a certain intrinsic interest, but would emphasize that they are much more tentative than the heavy ion reactor as discussed. They are as follows:

(1) No absolute limit on the potential achievable in these devices has been ascertained, though the requirements in terms of size and magnetic-field strength increase as the potential increases. At  $5 \times 10^8$  V or so a clashing-beam meson factory becomes a possibility, although highly preliminary calculations indicate that this machine does not have any special advantages as compared with the proposed LASL meson factory.<sup>10</sup>

(2) At energies over 1 BeV, accelerated protons are relativistic and the advantages of clashing-beam machines in terms of center-of-mass energy become an important consideration.<sup>11</sup> We are, however, up against a fundamental limitation. For such machines to be interesting the protons would have to acquire a speed at least as great as the  $E/B$  velocity, if not greater. Under adiabatic conditions it is impossible for the protons to acquire a speed greater than the  $E/B$  velocity. On the other hand, it *may* be possible to make the protons behave nonadiabatically (e.g., by excitation at an appropriate frequency). If this were the case, it would be possible to make a clashing beam machine for any energy. This possibility has not been investigated.

This survey of other possible applications of the HIPAC principle concludes our introduction. It cannot at present be stated with complete assurance that the HIPAC will work as hoped, or indeed that it will work at all. However, two years of effort on the subject

indicate that the chances of success are good. Sections II and III are an effort to explain the basis of this assessment. Appendices A, B, and C treat, respectively, an energy-loss mechanism that can be important where many successive ionizations are required, some remarks on possible methods of nuclear diagnostics that might be applied to the HIPAC, and a brief indication of a way by which the desired time variation of the magnetic field (short rise time, long duration) might be achieved.

## II. ELECTRONIC EFFECTS

In this section we discuss certain basic features of the electron cloud, features which can be discussed without reference to the possible presence of ions. This approach allows us to separate the establishment of the potential well from its use as a tool for accelerating ions; it also corresponds to the natural experimental approach to the HIPAC. The features of the electron cloud to be discussed in this light are equilibrium, establishment, and stability. Discussion of these subjects on an "ideal" basis, that is, ignoring all loss mechanisms, allows us to calculate in a general way important parameters for HIPAC's of different sizes. These calculations, and a more detailed calculation for a 20 cm, 26 kG HIPAC are given in Part 4 of this section. Consideration of multiple ionization and of the losses due to collisional, radiative, and other processes is deferred until Sec. III.

### 1. Equilibrium

The discussion of the equilibrium in the HIPAC is simplified by separating it into two parts. First we discuss the equilibrium of an infinite cylindrical system; the cross section of this system will closely resemble a meridional section of the toroidal HIPAC. Second, we discuss the effect on equilibrium of the toroidal shape of the true HIPAC.

Suppose the infinite cylindrical system is filled to uniform density  $n_e$  with electrons. The radial electric field  $E_r$  will increase linearly from zero on the axis to  $n_e ea/2\epsilon_0$  at the wall (radius  $a$ ). If the magnetic field  $B$  is assumed unaffected by the electron current, the azimuthal drift velocity  $E_r/B_z$  will also increase linearly with radius, going from zero on the axis to  $n_e ea/2\epsilon_0 B$  at the wall. This corresponds to a "solid-body" rotation of the entire electron cloud with angular velocity

$$\frac{1}{2} \frac{n_e e}{\epsilon_0 B} = \frac{1}{2} \frac{\omega_p^2}{\omega_c} = \frac{1}{2} q \omega_c, \quad (\text{II.1.1})$$

where

$$q \equiv \frac{\omega_p^2}{\omega_c^2} = \frac{n_e m_e c^2}{B^2 / \mu_0}. \quad (\text{II.1.2})$$

Taking the potential of the axis as zero, the potential increases parabolically with radius, reaching the value  $n_e ea^2/4\epsilon_0$  at the wall.

<sup>10</sup> Meson Factories, Report of Ad Hoc Panel to the Office of Science and Technology, 1964 (unpublished).

<sup>11</sup> G. S. Janes, R. H. Levy, and H. E. Petschek, Phys. Rev. Letters **15**, 135 (1965).

The ratio  $q$  is a number of particular importance in the theory of crossed-field electron beams. It has the value unity when the magnetic energy per electron is about 250 keV. In the HIPAC,  $q$  will generally be much less than unity ( $\sim 0.001$  to  $0.05$ ) so that the magnetic energy per electron will range from 5 to 250 MeV. A different interpretation of  $q$  is the ratio of the centrifugal force on an electron to the electric or magnetic force. When  $q$  is small, the centrifugal force (in the large "drift" orbit, not the small Larmor orbit of Fig. 4) is negligible compared to the electric and magnetic forces which are closely balanced. It is just when these forces are balanced that we can neglect the electron inertia and write for the electronic equation of motion

$$\mathbf{E} + \mathbf{v}_e \times \mathbf{B} = 0. \quad (\text{II.1.3})$$

The drift velocity  $E/B$  is, of course, the solution of this equation for  $v_e$ . One more interpretation of  $q$  is of significance. Let us calculate the ratio of the so-called electron magnetron radius  $r_e$  (i.e., the Larmor radius at the  $E/B$  speed) to the size  $a$  of the system. We find

$$\frac{r_e}{a} = \frac{m_e(E/B)}{eBa} = \frac{m_e n_e e}{eB^2 2\epsilon_0} = \frac{1}{2}q. \quad (\text{II.1.4})$$

Note that this derivation depends on the fact that the entire electric field is due to space charge, i.e., that the electric field is not applied by means of external electrodes. Finally,  $q$  is approximately the ratio between the kinetic and potential energies of a typical electron.

In the equilibrium described above the electrons can be described as "cold," that is, they participate in the directed motion associated with solid-body rotation. They may also have a "thermal" motion which would consist of Larmor orbits of a certain size superposed on the general rotation. Such a thermal motion would not affect the equilibrium condition. Note that this equilibrium is fundamentally different from the equilibrium postulated for the  $E$  layer in the Astron.<sup>12</sup> In the Astron the electric force is negligible, and equilibrium is established by balancing magnetic and inertial forces. The drift velocities contemplated for the HIPAC correspond to electron energies in the range 10–100 keV. This compares with 5 MeV or so for the Astron.

The assumption of uniform electron density made above is by no means necessary. Equilibrium is present for arbitrary variation of density with radius, although in general the rotation will be more complicated than solid body and certain configurations are known to be unstable.

The electron motion produces currents which tend to reduce the magnetic field at the axis of the HIPAC. This effect can be estimated quantitatively as follows

<sup>12</sup> N. C. Christofilos, in *Proceedings of 2nd U. N. Conference on Peaceful Uses of Atomic Energy* (United Nations, Geneva, 1958), Vol. 32, p. 279.

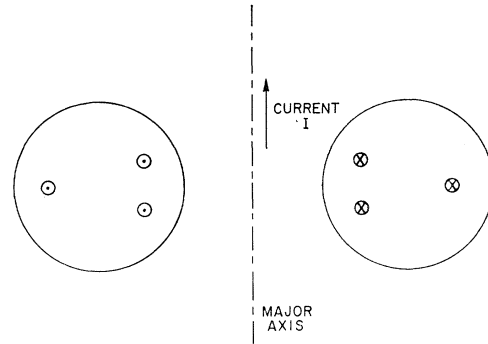


FIG. 7. This figure illustrates the essential decrease in magnetic field intensity across any section of the HIPAC. When the magnetic field is due to a current flowing along the major axis of the HIPAC, as illustrated (and returning at a large distance), the magnetic field is purely azimuthal, but decreases inversely with distance from the major axis.

from Maxwell's equations;

$$\Delta B / \Delta r \approx \mu_0 n_e v_e, \quad (\text{II.1.5})$$

$$v_e \approx E / B, \quad (\text{II.1.6})$$

$$\Delta E / \Delta r \approx n_e e / \epsilon_0. \quad (\text{II.1.7})$$

From these equations it is seen that

$$\frac{\Delta B}{B} \approx \left(\frac{v_e}{c}\right)^2 \frac{\Delta E}{E} \approx \left(\frac{v_e}{c}\right)^2, \quad (\text{II.1.8})$$

and hence that the reduction in magnetic field is not important until the electron drift velocity approaches the speed of light. More detailed investigation shows that as  $v_e \rightarrow c$  at constant magnetic-field strength (as, for example, by increasing  $E$  at the wall), the total potential across the system actually drops because of the necessity for removing charge from the center when the magnetic field there is practically annulled. As a result, there is a maximum potential attainable for a given magnetic-field strength and radius  $a$  which is of the form

$$V_{\max} = \text{const. } cBa. \quad (\text{II.1.9})$$

This maximum typically occurs for  $v_e/c$  around 0.7.

The above remarks all apply to equilibrium in infinite cylindrical systems. We now turn to consideration of equilibrium in toroidal systems where the situation is not as yet clear although some relevant remarks can be made. The basic fact is that in a toroidal geometry, the curl-free condition on  $B$  requires that the magnetic-field intensity decrease with distance from the major axis. This feature is easily seen to hold if the magnetic field in Fig. 7 is supposed due to a current flowing along the major axis of the device in which case we have  $B \propto 1/R$  where  $R$  is the distance of any point in the HIPAC from this axis. Now it is known from experience with stellarators<sup>13</sup> that static equilibrium in a simple toroidal geometry is impossible for a *neutral*

<sup>13</sup> L. Spitzer, Jr., *Phys. Fluids* 1, 253 (1958).

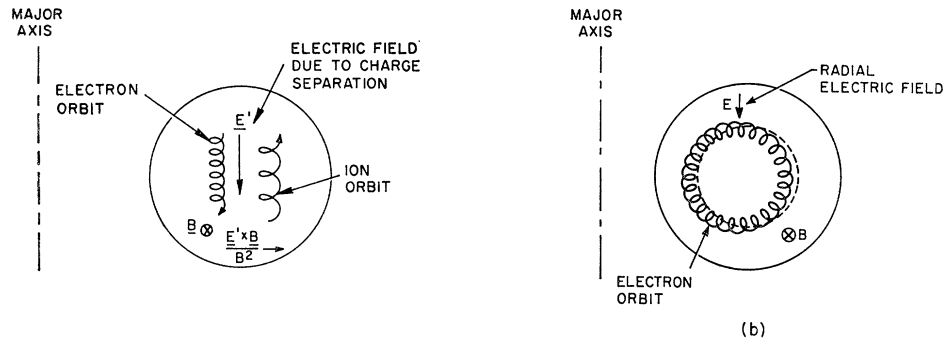


FIG. 8. This figure illustrates the effect of the gradient in the intensity of the magnetic field (as shown in Fig. 7) on the confinement of (a) a neutral plasma and (b) an electron plasma. Case (a) represents the situation as it would exist in a stellarator without rotational transform as shown. The electric field produced by charge separation leads to an  $E' \times B$  drift of the whole plasma to the outer wall, that is, to a region of lower  $B$ . In the case of the HIPAC [Fig. 8(b)] the situation is dominated by the space-charge electric field due to the electrons which is radial. This radial field produces a rotation of the electron cloud and appears to permit an equilibrium to exist without the necessity for a magnetic rotational transformation. There may also be a slight shift of the whole electron distribution towards the major axis. *Added in proof:* Highly preliminary toroidal experiments appear to support this point of view.

plasma, and this fact can be demonstrated from both the particle and the continuum points of view. In the first case, the inhomogeneity of the magnetic field produces a drift which will be down for the electrons if it is up for the ions [see Fig. 8(a)]. The charge separation that results then produces an electric field parallel to the major axis which causes the entire plasma to drift outwards, away from this axis. This is the particle view of the desire of the plasma to squeeze itself out of regions of high magnetic field and expand into a region of lower magnetic field. The same tendency has been elegantly derived from the continuum viewpoint by Yoshikawa,<sup>14</sup> who makes use of the virial theorem.

For the stellarator, which is supposed to contain a neutral plasma, this effect is overcome by the "rotational transform."<sup>13</sup> We need not describe this technique here, however, since it is not at all clear that any such complications are required for the HIPAC.

We observe first that the addition of a radial electric field (that is, an electric field of the type contemplated in the HIPAC) has been shown both experimentally<sup>15,16</sup> and theoretically<sup>17-19</sup> to reduce particle losses in the stellarator. From the particle point of view it can be seen (as shown by Bishop<sup>17,18</sup> and Budker<sup>19</sup>) that the rotating motion produced by the electric field tends to cancel out the *net* particle drift—upward or downward—that would otherwise be present. This is illustrated in Fig. 8(b). Instead, the circular (equipotential) tra-

jectory that would be present if the magnetic field were uniform is slightly shifted towards the major axis but—and this is the essential point—it remains closed, or cyclic, and therefore does not lead to a loss of the particles to the walls. A slight distortion or shift of the orbit is, of course, of no consequence.

This apparent stabilizing effect of a radial electric field has not yet been thoroughly analyzed from the continuum viewpoint; a calculation performed by the authors appears to give the same result as that obtained by Budker,<sup>19</sup> but is still in too preliminary a stage to be regarded as a proof. On the other hand, Yoshikawa's method<sup>14</sup> of using the virial theorem to demonstrate the impossibility of a simple toroidal equilibrium for a neutral plasma definitely breaks down when an important electric force is present; thus, the virial theorem cannot be used to show that equilibrium in the HIPAC is impossible.

In the HIPAC it is proposed to use an electric field vastly stronger than anything contemplated or possible in the stellarator. Thus, the effects of a radial electric field—already shown both experimentally and theoretically to be favorable—can be expected to be of great importance in the toroidal equilibrium of the HIPAC.

In somewhat more general terms, it can be argued that one would expect to be able to contain a *charged* electron plasma in a torus. This is because of the importance of forces due to the image charges; these forces cause the electrons to rotate and this rotation tends to cancel any net upward or downward drift. This argument may refer more to stability than to equilibrium, but seems reasonable in either case. In the end, however, while the situation looks hopeful, the answer to the problem of containment in toroidal systems is not yet known, and this problem is one of many which urgently need further experimental and theoretical study.

<sup>14</sup> S. Yoshikawa, *Phys. Fluids* **7**, 278 (1964).

<sup>15</sup> J. G. Gorman, *Bull. Am. Phys. Soc.* **10**, 195 (1965).

<sup>16</sup> J. G. Gorman and L. H. Th. Rietjens, *Plasma Physics Laboratory, Princeton University, Princeton, New Jersey, MATT-346, 1965* (unpublished).

<sup>17</sup> A. S. Bishop and C. G. Smith, *Bull. Am. Phys. Soc.* **10**, 23 (1965).

<sup>18</sup> C. G. Smith and A. S. Bishop, *Bull. Am. Phys. Soc.* **10**, 23 (1965).

<sup>19</sup> G. I. Budker, in *Plasma Physics and the Problem of Controlled Thermonuclear Reactions*, edited by Academician M. A. Leontovich (Pergamon Press, Inc., New York, 1961), Vol. I, p. 78.

2. Establishment

As in all machines in which charged particles are required to move adiabatically on closed orbits, particle injection is a problem needing careful attention. For the HIPAC the difficult part of the injection procedure is to get the electrons into their positions; once this has been done, ion injection should not pose any problem. A workable method of electron injection has been suggested and demonstrated experimentally at low (~10-kV) voltage. No reason is known why the same method will not operate well at much higher voltages.

This procedure, called inductive injection, depends upon introducing the electrons near the outer wall of the HIPAC while the magnetic field is rising to its desired value. When the magnetic field has reached its final value, injection is completed and (apart from losses) the whole device could be maintained indefinitely at this condition as long as the magnetic field is maintained. Some additional comments on how this mode of operation might be achieved are given in Appendix C.

The principle of inductive injection can be viewed from several angles. We can consider that an electron, once placed on a given flux surface, will subsequently follow the motion of this flux surface, provided that it moves sufficiently slowly. As the magnetic field increases, the flux surfaces are compressed towards the circular axis of the HIPAC, thus carrying the electrons away from the wall. In carrying the electrons away from the wall, the electrostatic field is energized. The source of this energy is in the capacitor bank energizing the magnetic field. An alternative view is to observe that as the magnetic field increases, an induced electric field will appear in the azimuthal direction (Fig. 9). Electrons experiencing this electric field will (by virtue of the presence of the magnetic field) drift radially inward at right angles to both fields. This direction of drift corresponds to the direction of the Poynting or power flow vector, and agrees with the idea that magnetic field lines are "born" near the windings, i.e.,

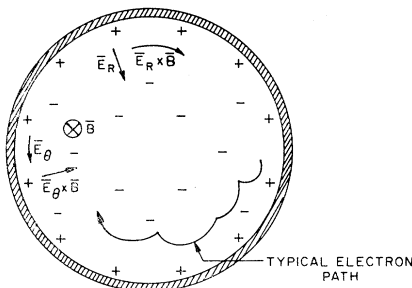


FIG. 9. Illustrates the principle of inductive charge injection. When the magnetic field is steady the only electric field is the radial field  $E_r$  due to space charge, and the only drift is the azimuthal drift  $E_r/B_z$ . When  $B$  is time varying, an induced azimuthal electric field appears,  $E_\theta = r\dot{B}/2$ , at radius  $r$ . This electric field yields a radial drift speed  $E_\theta/B_z = r\dot{B}/2B$ . This drift is inwards when  $B$  is increasing and vice versa. Since this speed will normally be small compared to  $E_r/B_z$ , the electron paths will resemble tightly wound spirals, as shown in Fig. 10.

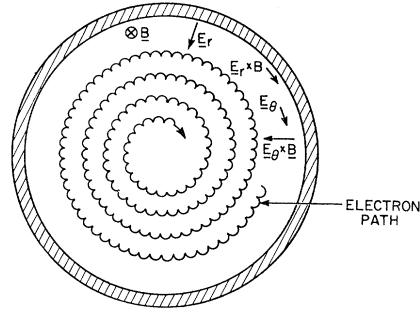


FIG. 10. The tightly wound spiral electron orbits which result from the inductive injection process are illustrated in this figure. In practice, the spiral would be much tighter than that shown here. Electrons follow the spiral trajectories inward when  $B$  is increasing and vice versa.

outside the HIPAC and are then carried away from the coils towards the axis of the device as the field strength rises.

The above remarks can be made quantitative as follows: when the magnetic-field strength varies temporally, there appears an azimuthal induced electric field which must satisfy

$$r \int_0^{2\pi} E_\theta(r, \theta) d\theta = -\frac{d}{dt} \int_0^r 2\pi r B dr. \quad (II.2.1)$$

There is, therefore, an average azimuthal electric field  $\vec{E}_\theta$  given by

$$\vec{E}_\theta = -\frac{1}{2}r\dot{B}. \quad (II.2.2)$$

For simplicity,  $B$  has been assumed spatially uniform. An electron making a circuit of the circular axis of the HIPAC at radius  $r$  is subject to this average accelerating electric field. Instead of simply causing the electron to move faster in its existing orbit, the electric field  $\vec{E}_\theta$  produces a radial drift in the direction perpendicular to  $\vec{E}_\theta$  and to  $B$ . The average speed associated with this drift,  $\vec{u}$ , is given by

$$\vec{u} = \vec{E}_\theta/B = -\frac{1}{2}r(\dot{B}/B), \quad (II.2.3)$$

where the minus sign indicates radially inward motion when  $\dot{B}$  is positive. The work done by the electric field  $E_\theta$  increases the potential, but not the kinetic energy of the electrons. The velocity  $\vec{u}$  can also be interpreted as the radial "velocity of the field lines" (see Longmire<sup>20</sup> for a discussion of this notion).

The net motion of the electrons in the presence of the radial and azimuthal electric fields is illustrated in Fig. 10. It consists of a very rapid azimuthal drift at the speed  $E_r/B$ , and a very slow radial inward drift at the speed  $\vec{E}_\theta/B$ . The combination of these motions is a tightly wound spiral orbit, as shown.

Equation (II.2.3) for the electron velocity is, of course, an adiabatic approximation, but will be valid

<sup>20</sup> C. L. Longmire, *Elementary Plasma Physics* (Interscience Publishers, Inc., New York, 1963).

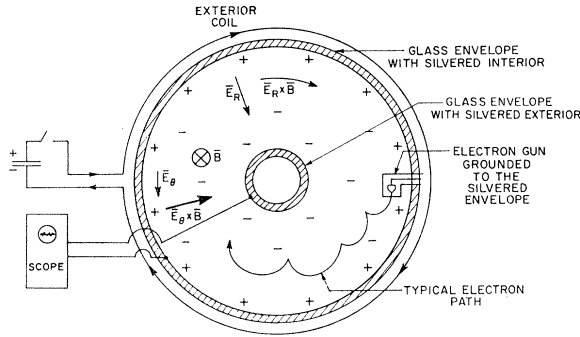


FIG. 11. This figure illustrates an early experimental test of the inductive charging concept. This experiment was straight (rather than toroidal) and had insulators at the ends of the cylinder. There was also an inner concentric cylinder of the same length whose sole purpose was to facilitate the measurement of the electrostatic potential between the axis and the outer cylinder. The outer cylinder was lightly silvered on the inside, and the inner cylinder was lightly silvered on the outside so that the magnetic field could penetrate both surfaces. Electrons were injected by a small gun firing, as shown in the direction of the  $E_r/B_z$  drift. The electrons were then carried inward by the rising magnetic field, those emitted early in the cycle being collected on the inner cylinder. Typical experimental results obtained with this apparatus are shown in Fig. 12.

as long as the characteristic time for compression of the magnetic field ( $B/\dot{B}$ ) is greater than the electron cyclotron period—a condition virtually impossible to violate in practice.

To see how the motion described by (II.2.3) distributes the electrons, we write an equation of continuity for the electrons, assuming azimuthal symmetry. This is

$$\frac{\partial n_e}{\partial t} + \frac{1}{r} \frac{\partial}{\partial r} (n_e r u) = 0. \quad (\text{II.2.4})$$

This equation ignores the rapid azimuthal drift motion of the electrons. This azimuthal drift is normally at a speed far greater than  $u$ , but, for reasons of symmetry, it does not contribute to the equation of continuity. Substituting for  $u$  from (II.2.3), and assuming that  $B$  (and hence  $\dot{B}$ ) is approximately uniform in space, we find

$$\frac{\partial n_e}{\partial t} - \frac{1}{2r} \frac{\dot{B}}{B} \frac{\partial}{\partial r} (n_e r^2) = 0. \quad (\text{II.2.5})$$

This equation has the general solution

$$n_e(r,t) = B(t) f[r^2 B(t)], \quad (\text{II.2.6})$$

where  $f$  is an arbitrary function. The physical meaning of this equation is that  $r^2 B(t) = \text{constant}$  is the characteristic trajectory (in space and time) of a flux surface, and that the quantity  $n_e/B$  is conserved as this surface moves about. The arbitrariness of the function  $f$  has to do with the value of  $n_e/B$  established by the electron injection system (whatever this may be—see below) at the wall  $r=a$  of the HIPAC. Assuming

injection to take place uniformly in the axial (magnetic field) direction, and neglecting azimuthal asymmetries in the injection process, the total injection current  $I$  is just

$$I(t) = 2\pi a l n_e(a,t) u(a,t). \quad (\text{II.2.7})$$

$l$  is the total length of the injection system, and might be equal to  $2\pi R$ , the major perimeter of the HIPAC. Substituting for  $u$  from (II.2.3), we find

$$I(t)/e l \pi a^2 \dot{B} = f[a^2 B(t)]. \quad (\text{II.2.8})$$

This equation shows how the function  $f$  is determined by the ratio of the injection current to the total induced electromotive force around a meridional section of the HIPAC;

$$\dot{\Phi} = \pi a^2 \dot{B}. \quad (\text{II.2.9})$$

The left-hand side of (II.2.8) is indeed the ratio of  $I/e l$  (the number of electrons per unit time per unit axial length entering the system) to  $\pi a^2 \dot{B}$ , which, in webers per second, is the rate at which flux lines are entering the system. In this way the ratio represents the number of charges per unit axial length per flux line, or the number of electrons actually placed on each field line as it passes into the HIPAC. This ratio is (as a function of time) to a large extent under our control. Suppose, as a simple example that we inject in such a manner as to maintain  $I/\dot{B}$  a constant. The function  $f$  is then a simple constant. From (II.2.6) this implies that the electron density is then at all times uniform in space, but that the level increases with time as the magnetic-field strength increases.

An interesting conclusion can be drawn from the description (II.2.6) of the compression process. The quantity  $q$  is proportional to  $n_e/B^2$ , whereas  $n_e/B$  is conserved for each parcel of electrons. It follows that

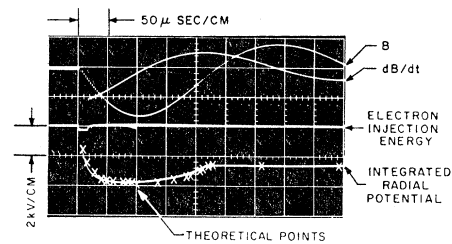


FIG. 12. A typical oscillogram obtained with the apparatus illustrated in Fig. 11. In the upper half, the traces show  $B$  and  $\dot{B}$ ; the quarter-cycle time was  $100 \mu\text{sec}$ . The trace near the axis shows the voltage applied to the electron gun; this was about  $200 \text{ V}$  for  $15 \mu\text{sec}$ . The lowest trace shows the variation of the potential between the inner and outer cylinders. A maximum of  $4 \text{ kV}$  was achieved, representing a voltage multiplication ratio of 20. More importantly, the distribution of electrons at different times was calculated assuming ideal adiabatic motion. At each instant of time, the distribution was integrated to give the radial potential; account was taken of the collection by the inner cylinder of electrons whose field lines were compressed inside it. These calculations are indicated by crosses, and are in excellent agreement with the experimental data. The residual potential at the end of the experiment represents the electrons collected by the inner cylinder.

the value of  $q$  for each parcel of electrons decreases by the same factor by which  $B$  increases. This is convenient, since injection may take place at a value of  $q$  not much less than unity, whereas it is desired that  $q$  should be roughly between 0.001 and 0.05 in the final state.

Although we have, in the preceding paragraphs, brought up the subject of electron injection, the subject has been treated only in generalities. We now consider the process in somewhat finer detail. We note first that the distribution of  $E_\theta$  around the cylinder may or may not be uniform. If the wall thickness of the HIPAC is small compared to the skin depth (at the frequency associated with  $\dot{B}/B$ ),  $E_\theta$  will be equal to  $\dot{E}_\theta$  uniformly around the circumference. This was the basis of early experiments on injection; these experiments are illustrated in Figs. 11 and 12. They involved the use of an electron gun inside the HIPAC, however, and, while they were reasonably successful as a first try, this method of injection has since been abandoned in favor of something much more elegant.

The new method involves making the wall of the HIPAC out of a good conductor, and then splitting the cylinder to make a slot, as shown in Fig. 13. In this arrangement the cylinder is an equipotential, so that the induced electromotive force  $\dot{\Phi} = \pi a^2 \dot{B}$  all appears across the slot, which can be quite narrow. All the field lines now enter the system through the slot, and electrons may be placed on them as they pass through. This method has the obvious advantage of leaving the interior of the HIPAC entirely clear of obstructions. This method has been successfully demonstrated, and an experimental oscillogram is shown in Fig. 14.

In general, the development of techniques for injecting is an area that definitely requires attention to the details of design, but which does not appear to reveal any insuperable problems. The problems are closely related to the problem of injecting into a

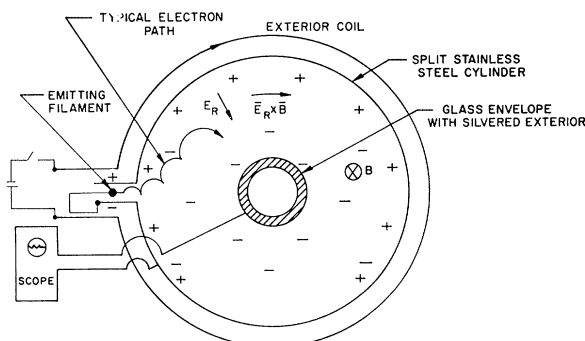


FIG. 13. This experiment is similar to that illustrated in Fig. 11, except that the outer cylinder is now solid metal (i.e., thick compared to the skin depth at the frequency  $\dot{B}/B$ ), and it is slotted. The entire induced electromotive force  $\pi a^2 \dot{B}$  now appears across the slot. Hence, all magnetic field lines enter through this slot. The gun now consists of a long heated filament set well back in the slot; no additional electric fields are applied. Results obtained with this apparatus are illustrated in Fig. 14.

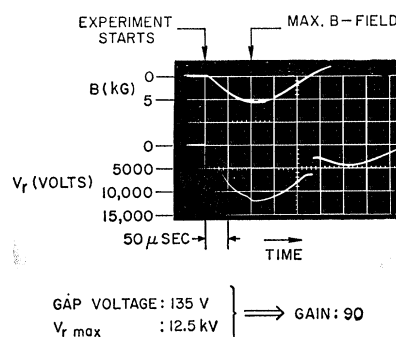


FIG. 14. Results obtained with the apparatus of Fig. 13. The upper trace is  $B$ ; it peaks at about  $100 \mu\text{sec}$ . The lower trace is the potential between the cylinders. The maximum gap voltage (induced by  $B$ ) was 135 V, the peak voltage between the cylinders was 12.5 kV, yielding a gain of about 90. The traces have no significant interpretation after the magnetic field declines to zero due to the occurrence of discharge on the insulating end plates. A simple estimate of the injection current and hence voltage history that this arrangement should yield has been made. The measured voltage history is in good agreement with this prediction.

magnetron which is reasonably well understood.<sup>21</sup> Quantitative differences remain, however, and the effect of these must be studied in detail. Among these are the requirement of the HIPAC that an injected electron acquire in the gun an energy not very much less than the energy it will have in  $E_r/B_z$  drift once it is inside the machine. Since the accelerating potential in the "gun" as shown in Fig. 13 is less than  $\pi a^2 \dot{B}$ , certain fairly stringent requirements are imposed on the rise time of the magnetic field. There may, however, be ways to avoid this difficulty by independent means.

The rise and decay times for the magnetic field need not be identical (nor even comparable). In a practical device we envision a short rise time for the magnetic field followed by a long period of substantially dc operation. Thus, a requirement for a very short rise time for the magnetic field would not preclude the possibility of long duration operating times. These ideas are discussed in greater detail in Appendix C.

### 3. Stability

Turning next to the problem of stability, we note first the existence of a large reservoir of potential energy all of which is readily available for driving any instability mechanism that may exist. A serious instability could cause the electric field to collapse in a microsecond or less, and render the HIPAC totally useless. As against this possibility, 2 years' experimental and theoretical work on this problem has yielded highly promising results.

An experiment was performed (Figs. 15, 16, and 17) in a geometry related to that of the HIPAC in which electrons were contained for over a million orbits; furthermore, the rate of loss of electrons (the anode

<sup>21</sup> G. S. Kino, in *Crossed-Field Microwave Devices*, edited by E. Okress (Academic Press Inc., New York, 1961), Vol. I, p. 164.

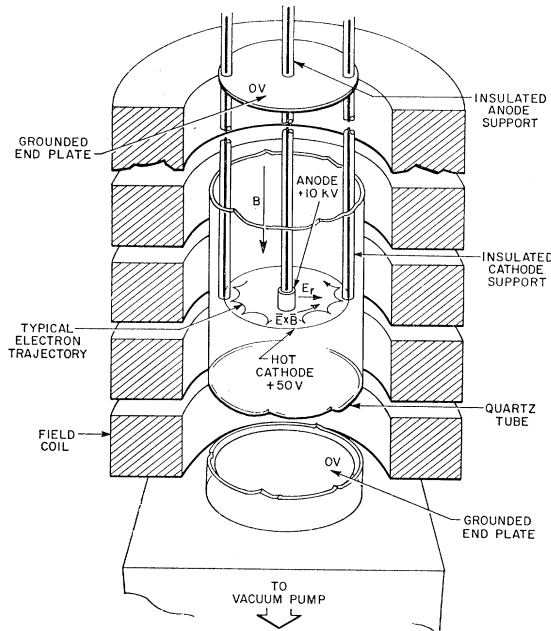


FIG. 15. This steady-state inverted magnetron-type experiment was performed with the object of studying the containment of electrons in crossed electric and magnetic fields. The geometry resembles that of the HIPAC except that it is linear rather than toroidal, and that the anode is at the center rather than at the outer wall. Electrons from a space-charge limited cathode are attracted to the anode by an applied potential of up to 10 kV. The anode current is then measured as a function of the applied magnetic field. The results are shown in Fig. 16.

current) scaled directly with background gas pressure indicating that the diffusion was entirely classical. The importance of this result lies in the observation that instabilities can easily be imagined with growth rates on the order of the circulation time; these evidently did not exist at least for the experiment actually performed. Of course, there might be one or more instabilities with much slower growth rates, but even if such instabilities did exist they should be easily controllable by feedback means. Feedback schemes have been used with success in particle accelerators to control unstable, slowly growing (radio-frequency) modes due to wall resistance.<sup>22-24</sup>

To be more precise on the question of instability, the basic driving mechanism for any interesting mode can be seen to reside in the electric field; in the presence of the electron cloud, however, the electric field has a nonvanishing divergence and this leads to a shear in the electron drift velocity. In a simple two-dimensional configuration as illustrated in Fig. 18, this shear or "vorticity" can be calculated as follows;

$$\omega_0 = \frac{du_y}{dx} = \frac{d(E_x/B_z)}{dx} = \frac{1}{B_z} \frac{n_e e}{\epsilon_0} \frac{\omega_p^2}{\omega_c} = q\omega_c. \quad (\text{II.3.1})$$

<sup>22</sup> R. A. Otte, H. Kamei, and C. H. Pruett, *Bull. Am. Phys. Soc.* **10**, 457 (1965).

<sup>23</sup> F. E. Mills, *Bull. Am. Phys. Soc.* **10**, 458 (1965).

<sup>24</sup> C. H. Pruett, F. E. Mills, and R. A. Otte, *Bull. Am. Phys. Soc.* **10**, 458 (1965).

[This formula is the two-dimensional analog of (II.1.1).] We observe that when  $q \ll 1$ , as happens in the cases of interest to us

$$\omega_0 \ll \omega_p \ll \omega_c. \quad (\text{II.3.2})$$

The basic instability of electron clouds having shear as above is called the "diocotron" or "slipping stream" instability<sup>25-29</sup> and forms the basis of the theory of the crossed-field microwave magnetron. While we do not intend to give a review of diocotron theory here, the following observations are worthwhile: in the presence of a uniform (static) magnetic field, and in the absence of collisions and other nonadiabatic effects the canonical momentum

$$p_y = mu_y - eA_y \quad (\text{II.3.3})$$

of each electron is conserved, and, furthermore, the same value of this momentum is conserved for each electron. We can therefore differentiate (II.3.3) in the  $x$  direction to obtain

$$\omega_0 = \omega_c. \quad (\text{II.3.4})$$

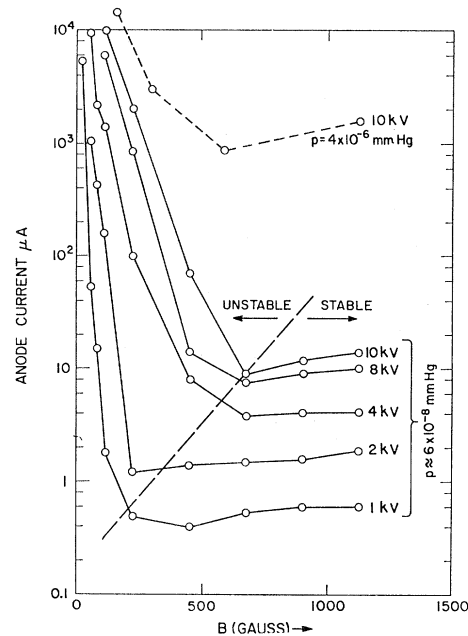


FIG. 16. Current-magnetic field plots for the apparatus of Fig. 15. For low  $B$ , large anode currents were drawn and the experiment emitted considerable rf noise. For  $B$  larger than a critical value (dashed line) but at the same applied voltage, the current stabilized at a low level, and the experiment became very quiet. The final current scaled linearly with the background pressure indicating that the anode current was principally due to classical diffusion. The interpretation of these results is given in Fig. 17.

<sup>25</sup> G. C. MacFarlane and H. G. Hay, *Proc. Roy. Soc. (London)* **63**, B409 (1953).

<sup>26</sup> O. Buneman, in *Crossed-Field Microwave Devices*, edited by E. Okress (Academic Press Inc., New York, 1961), Chap. 5.

<sup>27</sup> R. W. Gould, *Tech. Rept. No. 3, Electron Tube and Microwave Laboratory, California Institute of Technology, 1965* (unpublished).

<sup>28</sup> B. Epsztajn, *Compt. Rend.* **240**, 408 (1955).

<sup>29</sup> O. Buneman, *J. Electronics* **3**, 1 (1957).

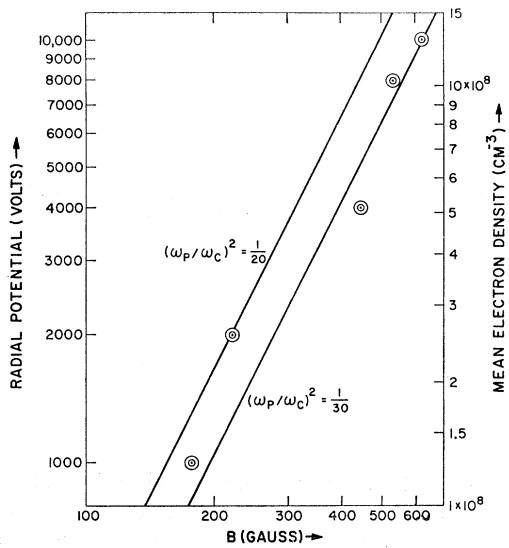


FIG. 17. A cross plot of the critically stable points from Fig. 15. The electron density was estimated from the applied voltage, the dimensions of the system, and the knowledge that the cathode was space-charge limited. Evidently stability is present for  $q = \omega_p^2/\omega_c^2 \leq 0.05$ . A theory exists (Ref. 4) which explains this phenomenon.

It follows from (II.3.1) and (II.3.4) that

$$q = 1, \text{ or } \omega_0 = \omega_p = \omega_c. \quad (\text{II.3.5})$$

Since the above conditions are thought to apply to magnetrons, it is for the special case  $q=1$  that the diocotron theory has been developed. The state described by  $q=1$  is often called the "Brillouin state." On the other hand, we have seen that we require  $q \ll 1$  in the HIPAC, and we have also seen how such values of  $q$  are attained in the injection process. A different, though analogous, way of viewing this effect is to note that by injecting later electrons into a higher magnetic field, each electron acquires a different value of  $p_y$ , so that the differentiation leading to (II.3.4) is invalidated.

The extension of magnetron theory to values of  $q \ll 1$  was undertaken. The results of this extension were as follows: for  $q=1$  (magnetron case) two classes of waves propagating in the drift direction are unstable; those having wavelengths long compared to the thickness of the electron beam, and those having wavelengths short compared to the same thickness. The growth rates of both classes of waves are on the order of any of the frequencies  $\omega_0$ ,  $\omega_p$ , and  $\omega_c$  (which are all equal in this case).

For  $q \ll 1$ , both classes of waves are still found to be unstable. However, the growth rate of the short waves is on the order of  $\omega_0 e^{-2/q}$ . For  $q \leq 0.05$  this growth is so slow as to be essentially unobservable in time scales of interest.<sup>4</sup> These waves, therefore, are not a problem for us. The long waves also remain unstable, and grow in times like  $\omega_0^{-1}$ . For  $q \ll 1$ , these waves closely resemble the waves causing the so-called Kelvin-Helmholtz

instability of fluid mechanics.<sup>30,31</sup> We can dispose of them by observing that the electron drift orbits are periodic; the longest permissible wavelength in the drift direction is just the length of the drift orbit. If the electron beam is thick relative to the length of the drift orbits, there may be no possibility of fitting in an unstable wave. Further stabilization against long waves is provided by the proximity of conducting walls. The remarks above are based on detailed quantitative analyses of these phenomena,<sup>3,32</sup> and also appear to be in qualitative agreement with experimental observations made both by the authors (Figs. 15, 16, and 17) and by others. The theoretical discussion is summarized in Figs. 19, 20, and 21. The essential point is that while the magnetron instability exists by virtue of an inherent instability of crossed-field electron beams, it is possible, by appropriate selection of parameters, to construct crossed-field electron beams which exhibit a considerable degree of stability. It is further possible to suggest theoretical reasons for this stability. Knauer<sup>33,34</sup> quotes evidence of crossed-field electron beams having electron containment times up to 15 sec.

The exhibition of control over the basic diocotron instability modes is of considerable importance, since it is thought that these modes have intrinsically the highest growth rates. It does not, however, exhaust the list of possible instabilities. Several other possible modes of instability have been investigated theoretically, some superficially, some in fair detail. Undoubtedly others still remain to be found. The difficulty at present lies in deciding which of the possibilities to investigate in detail, in the absence of firm experimental evidence of any instability. In spite of this situation, some of the modes considered will be briefly described here:

First, residual resistance in the walls will undoubtedly cause an instability to appear.<sup>35-37</sup> On the other hand, for reasonable parameters, the growth rate of this instability should be quite low, namely less than the fraction  $(\omega_0 \epsilon_0 / \sigma)^{1/2}$  of the growth rate associated with the diocotron modes. For the example quoted in the next section,  $\omega_0 \approx 10^9 \text{ sec}^{-1}$ , and for copper with  $\sigma / \epsilon_0 \approx 6.55 \times 10^{18} \text{ sec}^{-1}$ , we obtain a growth rate less than  $1.25 \times 10^4 \text{ sec}^{-1}$ . One would expect to control a slow growth of this type with some form of feedback system analogous to that used in particle acceler-

<sup>30</sup> S. Chandrasekhar, *Hydrodynamic and Hydromagnetic Stability* (Clarendon Press, Oxford, England, 1961).

<sup>31</sup> C. C. Lin, *The Theory of Hydrodynamic Stability* (Cambridge University Press, New York, 1955).

<sup>32</sup> R. H. Levy and J. D. Callen, *Phys. Fluids* **8**, 2298 (1965).

<sup>33</sup> W. Knauer and E. R. Stack, in *Transactions of the Tenth National Vacuum Symposium, Boston, 1962* (The Macmillan Company, New York, 1963), p. 180.

<sup>34</sup> W. Knauer, *J. Appl. Phys.* (to be published).

<sup>35</sup> O. Doehler and Gorges Guilbaud, *Compt. Rend.* **238**, 1784 (1954).

<sup>36</sup> Iwao, Sugai, and G. Mourier, Polytechnic Institute of Brooklyn, Electrophysics Group, Memorandum No. 30, 1957 (unpublished).

<sup>37</sup> C. K. Birdsall, G. R. Brewer, and A. V. Haef, *Proc. I.R.E.* **41**, 865 (1953).

## PLANAR ELECTRON BEAM

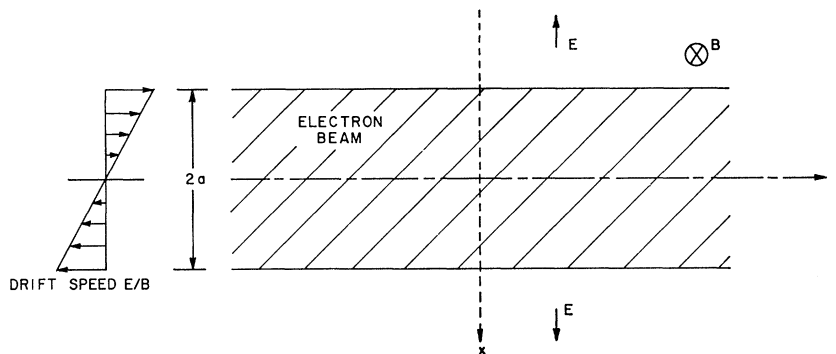


FIG. 18. Illustration of the inherent presence of shear in crossed-field electron beams.

ators.<sup>22-24</sup> The use of such schemes with charged beams is in principle not at all difficult. This contrasts with the situation in neutral plasmas where applied electric fields are screened out by the plasma within a Debye length.

A related mechanism of instability has to do with the possible destabilizing effect of coherent radiation on the electron cloud. This possibility has been studied in detail<sup>38</sup> for the geometry of the plasma radiation shield,<sup>39</sup> where it appears that the impedance of free space acts somewhat like a resistive wall facing the electron beam, and can in fact excite an instability. For the HIPAC, radiation directly to infinity cannot take place in view of the conducting (i.e., reflecting) wall. Viewed as a waveguide, the HIPAC is "cut off" at the frequencies possible for the electron cloud. It therefore seems likely that no radiative instability need be expected in the HIPAC. This point, however, cannot as yet be regarded as finally settled. It is of importance to the HIPAC to settle it because radiative effects of this type are certainly enhanced when the electron speed approaches the speed of light and, as we have seen, we are tempted to make it do just this, both to economize on magnetic field, and to give the electrons sufficient energy to ionize. Apart from radiation, there

may very well be other important relativistic effects on stability resulting from the high electron speeds contemplated, but no knowledge of the nature of these presently exists.

The same lack of knowledge exists in all other aspects of the stability problem. Even though we can give a list of some possibilities, no reliable estimate of the importance of any item in it can be made. This situation is likely to prevail until experimental indications of instability come to hand. Possible sources of interesting instabilities are:

(1) Effects associated with the motion of electrons along magnetic-field lines. All theories to date (and this includes the theories which underlie the magnetron) ignore this effect which may be of importance in determining allowable major to minor axis ratios for the HIPAC.

(2) Effects of a thermal spread in electron velocity. The same comment about magnetron and other work applies here, too.

(3) Toroidal effects on stability, as opposed to the toroidal effects on equilibrium discussed earlier in this section.

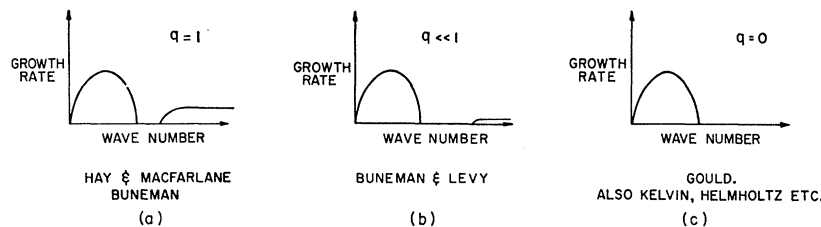


FIG. 19. Schematic diagram of growth rate versus wave number for waves propagating in the drift direction for the geometry of Fig. 18. The maximum growth rate for the long waves is on the order of  $\omega_0 = \omega_p^2 / \omega_c$ . The wave number scale is such that the growth rate for the long waves vanishes for waves whose length is comparable to the beam thickness. For  $q (= \omega_p^2 / \omega_c^2) = 1$  (the magnetron case) growth is predicted for long and for short waves. For  $q \ll 1$  (HIPAC case) the growth of the long waves is unaffected, but the growth rate of the short waves is reduced to  $\omega_0 e^{-2/q}$ —a negligible number for  $q \lesssim 0.05$ . In the limit  $q = 0$ , the short-wavelength growth disappears altogether; the instability is then perfectly analogous to the Kelvin-Helmholtz instability of fluid dynamics with  $\omega_0$  representing the vorticity. For an explanation of how this long-wavelength instability is avoided in the HIPAC, see Figs. 20 and 21.

<sup>38</sup> R. H. Levy, *J. Appl. Phys.* **37**, 119 (1966).

<sup>39</sup> The plasma radiation shield is a topologically involuted version of the HIPAC intended for use in space. Described elsewhere (Ref. 50), its physical basis is essentially identical to that of the HIPAC.

4. Sample Calculation

The preceding material enables us to undertake a "sample calculation" whose object is to illustrate in detail the properties of a typical HIPAC. Before doing this calculation, however, some remarks on scaling laws are appropriate.

The electric field  $E$ , the total potential  $V$  and the minor radius  $a$  are related through

$$E \propto V/a, \tag{II.4.1}$$

the electron drift velocity is

$$v_e \propto E/B, \tag{II.4.2}$$

thus

$$V \propto av_e B \tag{II.4.3}$$

provided  $v_e \lesssim 0.7c$ . From Poisson's law we find

$$n_e \propto V/a^2. \tag{II.4.4}$$

The volume of the HIPAC,  $\mathcal{V}$ , is given by

$$\mathcal{V} \propto a^2 R \propto a^3 (R/a) \propto a^3 \tag{II.4.5}$$

if the radius ratio is fixed.

As a "clashing-beam" machine, the total reaction rate  $\mathcal{R}$  is given by

$$\mathcal{R} = \frac{1}{2} n_i^2 \sigma_{ii} v_i \mathcal{V}. \tag{II.4.6}$$

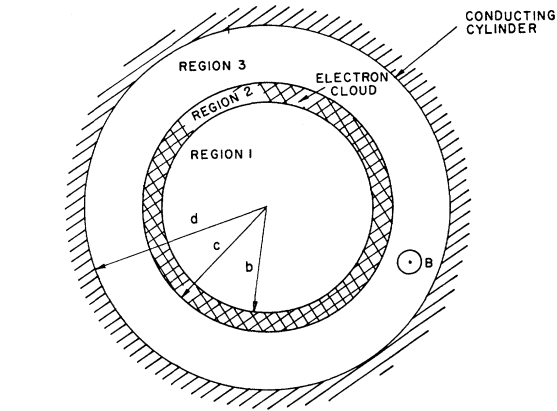


FIG. 20. We consider the geometry illustrated above for the case  $q \ll 1$ , so that only the long waves need be treated. Instead of having waves of arbitrary length propagating parallel to the drift direction (azimuthally), we now have mode numbers  $l=0, 1, 2$ , etc. A stability plot for these modes is given in Fig. 21.

With regard to the ion density, it is not at present very clear what values can be achieved. For the moment, we shall therefore make the following somewhat arbitrary assumption

$$n_i = \frac{1}{10} (n_e/Z). \tag{II.4.7}$$

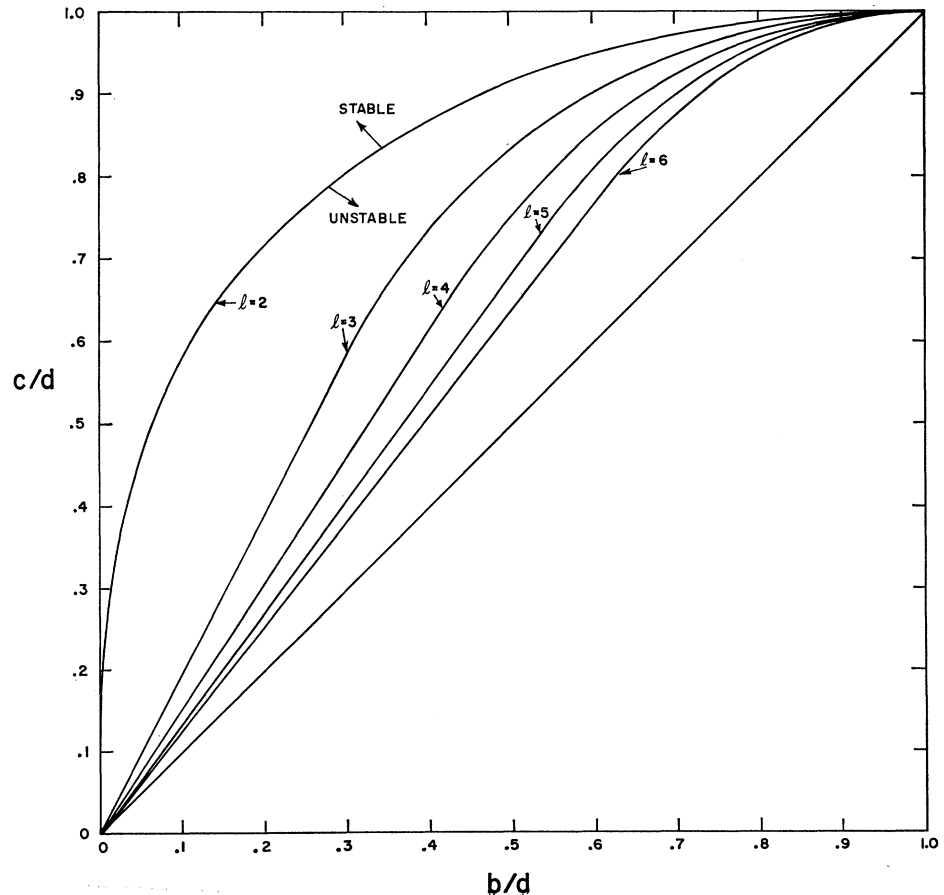


FIG. 21. A stability plot for the geometry of Fig. 20. The modes  $l=0$  and 1 are always neutrally stable in these cases, and the other modes exhibit stability or instability as shown. The mode  $l=2$  is clearly the most dangerous, but this mode (and hence all the others) can be stabilized by having the electron cloud thick enough or near enough to the outer wall.

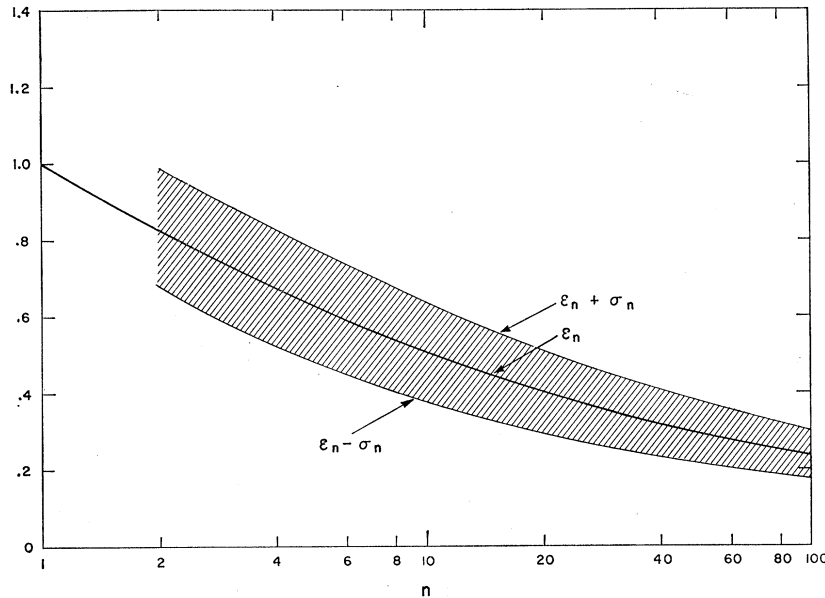


FIG. 22. A singly ionized atom released at rest at potential  $V_1$  will become highly stripped in the HIPAC. To become stripped, however, requires a time such that the atom will traverse its potential well a large number of times. After being ionized  $n$  times, its energy will generally be less than  $neV_1$  since some ionizations may have occurred at low potential; these ionizations reduce the depth of the well in which the particle oscillates from  $V_1$  to  $V_n \leq V_1$ . This figure shows the expectation  $\varepsilon(V_n) = \varepsilon_n$  (i.e., the average value of  $V_n$ ) and the standard deviation  $\sigma_n = \{\varepsilon(V_n^2) - [\varepsilon(V_n)]^2\}^{1/2}$ . It can be seen that after 90 or 100 ionizations most atoms will have well depths of  $V_n$  around  $\frac{1}{4}V_1$ , and will therefore have energies like  $\frac{1}{4}neV_1$ . The probability functions  $p_n(V)$  from which this figure is constructed are illustrated in Fig. 27, and the method of calculating them and the assumptions used are given in Appendix A. The fact that the ion is moving slowest, and therefore spends most of its time at high potential has been taken into account. The degree of ionization  $n$  is equivalent to the effective atomic number  $Z_{\text{eff}}$ .

This assumption guarantees that the ions are not sufficiently numerous to depress significantly the depth of the potential well. However, the effect of this quantity of ions on the stability of the electron cloud—treated hitherto as consisting solely of electrons—is not known. It is known that in the presence of net charge neutrality instabilities of various kinds can lead to an anomalous diffusion of the entire plasma. An important area of research will be the establishment of the stability boundary that apparently exists between pure electron plasmas on the one hand, and neutral plasmas on the other. In the absence of knowledge of this boundary, (II.4.7) will have to serve as a working hypothesis.

If the 10% neutralization assumption turns out to be appropriate, (II.4.7) may turn out to be conservative since it is not in principle necessary to have the heavy ions completely stripped. If a number  $Z_{\text{eff}}$  of electrons is removed from the atom, the resulting ionic charge is  $Z_{\text{eff}}e$ , and the 10% neutralization assumption should contain  $Z_{\text{eff}}$  instead of  $Z$ . The fundamental uncertainty of (II.4.7), however, renders such precision unjustified and, for lack of anything better we shall use (II.4.7) in the form stated.

With respect to the ion velocity, the following comment is of some importance; if every ionization took place at the outside wall, the energy of each ion would be  $Z_{\text{eff}}eV$ , where  $Z_{\text{eff}}$  is the number of electrons removed from a given atom. If the atomic number (nuclear charge) is  $Z$ ,  $(Z - Z_{\text{eff}})$  is the number of electrons remaining in inner Bohr orbits. An atom can be injected in a singly or doubly ionized state at the outside wall. Once injected, however, the ions accelerate rapidly and on the average cross the system many times before the occurrence of the next ionization. Thus, the second and succeeding ionizations have a reasonable probability of occurring near the center of the well with

a consequent reduction in the final ion energy. This effect which is probabilistic in nature is considered in detail in Appendix A where it is shown that for large  $Z_{\text{eff}}$ , it is equivalent to a reduction in the average ion energy by a factor  $1.1 Z_{\text{eff}}^{-1/3}$ . This result is also illustrated in Fig. 22 where the expected spread in ion energies is shown together with the average degradation. (In the Appendix the notation “ $n$ ” is used for  $Z_{\text{eff}}$ .)

These remarks make it clear that the typical ion velocity, for use in calculating the reaction rate (II.4.6), should be taken as

$$v_i \propto Z_{\text{eff}}^{1/3} V^{1/2} \tag{II.4.8}$$

provided (as is generally the case) that this velocity is less than the  $E/B$  velocity.

Collecting the previous formulas, we find that the total reaction rate varies as

$$R \propto \frac{V^{5/2} Z_{\text{eff}}^{1/3}}{a Z^2} \tag{II.4.9}$$

We conclude the collection of scaling laws by observing that the magnetic energy stored,  $U_B$ , varies as

$$U_B \propto B^2 a^3 \tag{II.4.10}$$

Since  $E/B \sim v_e$ , the stored electric energy

$$U_E \propto (v_e^2/c^2) U_B \tag{II.4.11}$$

With these scaling laws it is possible to consider a whole family of possible HIPAC's; from this family it would in principle be possible to choose an optimum design for any particular purpose. Such an optimization has not yet in fact been done, and instead, we shall consider a single machine as representative of the kind of thing that can be expected. The machine chosen will

TABLE I. Parameters of a typical HIPAC.

Geometrical		
Minor radius	$a$	20 cm
Major radius	$R$	100 cm
Volume	$\mathcal{V}$	$7.9 \times 10^5 \text{ cm}^3$
Electrostatic		
Voltage	$V$	$2 \times 10^7 \text{ V}$
Wall electric field	$E$	$2 \times 10^6 \text{ V/cm}$
Electron density	$n_e$	$1.1 \times 10^{11} \text{ cm}^{-3}$
Plasma frequency	$\omega_p$	$1.9 \times 10^{10} \text{ sec}^{-1}$
Number of electrons	$N_e$	$8.7 \times 10^{16}$
Electric field energy	$U_E$	$1.4 \times 10^6 \text{ J}$
Magnetic		
Magnetic field	$B$	26 kG
Cyclotron frequency	$\omega_c$	$4.6 \times 10^{11} \text{ sec}^{-1}$
Magnetic field energy	$U_B$	$2.1 \times 10^6 \text{ J}$
Flux	$\pi a^2 B$	0.33 Webers, i.e., V-sec
Electromagnetic		
$\omega_p^2/\omega_c^2$	$q$	$1.7 \times 10^{-3}$
$\omega_p^2/\omega_e$	$\omega_0$	$7.7 \times 10^8 \text{ sec}^{-1}$
Electron drift velocity	$v_e = E/B$	$7.7 \times 10^9 \text{ cm/sec} = 0.26c$
Electric/magnetic energy	$(E/cB)^2 = U_E/U_B$	0.066
Injection time	$\tau_{inj}$	20 $\mu\text{sec}$
Ions		
Number density	$n_i$	$1.1 \times 10^{10}/Z \text{ cm}^{-3}$
Number of ions	$N_i$	$8.7 \times 10^{15}/Z$
Electron drift energy		18 keV
Electron flux	$n_e v_e$	$8.5 \times 10^{20} \text{ cm}^{-2} \text{ sec}^{-1}$
Oscillation time in potential well	$\tau_{osc}$	$10^{-9} (A/Z_{eff})^{1/2} \text{ sec}$
Ion velocity (fully stripped)	$v_i$	$4.5 \times 10^9 \text{ cm sec}^{-1}$
Nuclear		
Total cross section (very rough)	$\sigma_{ii}$	$4 \times 10^{-25} Z^{2/3} \text{ cm}^2$
Volumetric reaction rate	$0.5 n_i^2 v_i \sigma_{ii}$	$1.1 \times 10^5 Z^{-4/3} \text{ cm}^{-3} \text{ sec}^{-1}$
Total reaction rate	$R = 0.5 n_i^2 v_i \sigma_{ii} \mathcal{V}$	$8.4 \times 10^{10} Z^{-4/3} \text{ sec}^{-1}$
Nuclear lifetime	$N_i/R$	$10^5 Z^{1/3} \text{ sec}$

have a minor radius

$$a = 20 \text{ cm} \quad (\text{II.4.12})$$

and major to minor radius ratio of 5:1

$$R = 100 \text{ cm}. \quad (\text{II.4.13})$$

The volume is then

$$\mathcal{V} = 7.9 \times 10^5 \text{ cm}^3. \quad (\text{II.4.14})$$

We choose the magnetic field strength to be

$$B = 26 \text{ kG}. \quad (\text{II.4.15})$$

This machine is therefore of quite modest proportions. The magnetic energy stored is

$$U_B = 2.1 \times 10^6 \text{ J}. \quad (\text{II.4.16})$$

We next choose the total voltage to be

$$V = 2 \times 10^7 \text{ V}. \quad (\text{II.4.17})$$

The purpose of this choice is to make clear that the highest voltages presently attainable can be reached in a HIPAC of quite small dimensions. Furthermore, exciting possibilities are available with this voltage which are not available either in Van de Graaff machines which can make voltages approaching this figure, or in other types of heavy ion accelerators. The voltage and

the radius  $a$  yield the characteristic electric field:

$$E = 2 \times 10^6 \text{ V/cm}. \quad (\text{II.4.18})$$

The electron density is

$$n_e = 1.1 \times 10^{11} \text{ cm}^{-3} \quad (\text{II.4.19})$$

and the value of  $q$  is

$$q = 1.7 \times 10^{-3}. \quad (\text{II.4.20})$$

The drift speed of the outermost electron is

$$v_e = 7.7 \times 10^9 \text{ cm/sec} = 0.26c. \quad (\text{II.4.21})$$

The drift (directed) energy of this electron is about 18 keV. The various frequencies in the electron cloud are

$$\omega_p = 1.9 \times 10^{10} \text{ sec}^{-1}, \quad (\text{II.4.22})$$

$$\omega_0 = 7.7 \times 10^8 \text{ sec}^{-1}, \quad (\text{II.4.23})$$

$$\omega_c = 4.6 \times 10^{11} \text{ sec}^{-1}. \quad (\text{II.4.24})$$

If 18 kV is to be generated across the slot in the torus (see the section on injection), the quarter-cycle time of the capacitor bank must be about 20  $\mu\text{sec}$ .

An important calculation shows that the effect of the magnetic field on the ions is negligible. At the  $E/B$  velocity the Larmor radius of a proton would be about

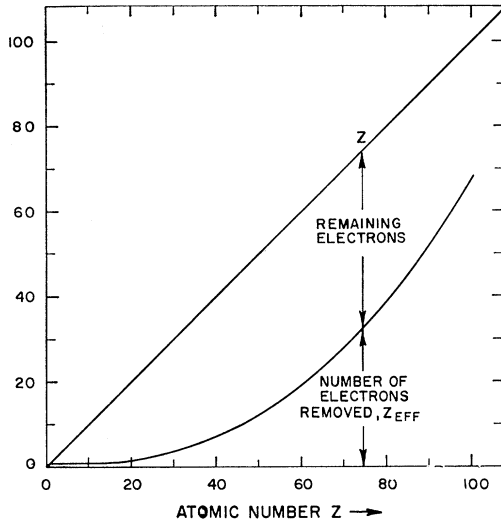


FIG. 23. For the HIPAC whose parameters are listed in Table II, a certain degree of stripping for heavy ions is required if these are to have sufficient energy to overcome the nuclear Coulomb barrier. This figure shows the number of electrons which it is required to remove from an atom of atomic number  $Z$  in order to accomplish this objective, taking into account the loss of energy associated with ionization at low potential, as calculated in Appendix A. Single ionization proves to be adequate for  $Z < 17$ , and complete stripping is not required for any ion. The ionization times shown in Fig. 24 and calculated in Sec. III are based on achieving the ionization state indicated on this figure.

30 cm, i.e., 1.5 times the radius of the containing vessel. In fact, in falling through  $2 \times 10^7$  V, a proton would pick up a velocity somewhat lower than the  $E/B$  velocity, but the conclusion still stands. For any heavy ion at all, the ratio of charge to mass is lower than for a proton, so that we may conclude that the effect of the magnetic field on the ion orbits is to cause these to precess slightly (Fig. 5), but that all the ions are magnetically free to fall through practically all of the available potential drop.

We can now view the HIPAC as containing a cloud of highly stripped ions oscillating backward and forward across the potential well. The number of reactions per second between the ions will be

$$\mathcal{R} = \frac{1}{2} n_i^2 \sigma_{ii} v_i = \frac{4.7 \times 10^{25}}{Z^2} \sigma_{ii} v_i. \quad (\text{II.4.25})$$

The factor  $Z^{-2}$  arises because the ion density is proportional (III.4.7) to  $Z^{-1}$ . The typical ion velocity will be in the range of a few times  $10^9$  cm/sec. Very roughly, then, the total number of reactions per second will be

$$\mathcal{R} = \frac{2.1 \times 10^{35}}{Z^2} \sigma_{ii}. \quad (\text{II.4.26})$$

The cross section  $\sigma_{ii}$  will naturally depend on exactly what reaction is of interest; however, if we assume in a very gross way that the cross section for some nuclear

reaction of interest is

$$\sigma_{ii} = \pi (2R_{\text{nuc}})^2 \approx 4 \times 10^{-25} Z^{2/3}, \quad (\text{II.4.27})$$

we find a total reaction rate

$$\mathcal{R} = 8.4 \times 10^{10} Z^{-4/3}, \quad (\text{II.4.28})$$

which is, however, divided among a number of competing reactions. The results obtained thus far are summarized in Table I.

It is of interest to compare this reaction rate to those available in conventional heavy ion accelerators. This we have done in Table II in which we have estimated the reaction rates available for various projectiles from a proposed high intensity cyclotron.<sup>6</sup> It is important to note that the ion currents assumed from this cyclotron are at least an order of magnitude, and in many instances several orders of magnitude, greater than those currently available. Nevertheless, we see that the best reaction rates for the heaviest available ions are not appreciably greater than those achievable in the relatively small HIPAC. As shown in Fig. 1, for reactions between heavier nuclei there is no competitor to the HIPAC.

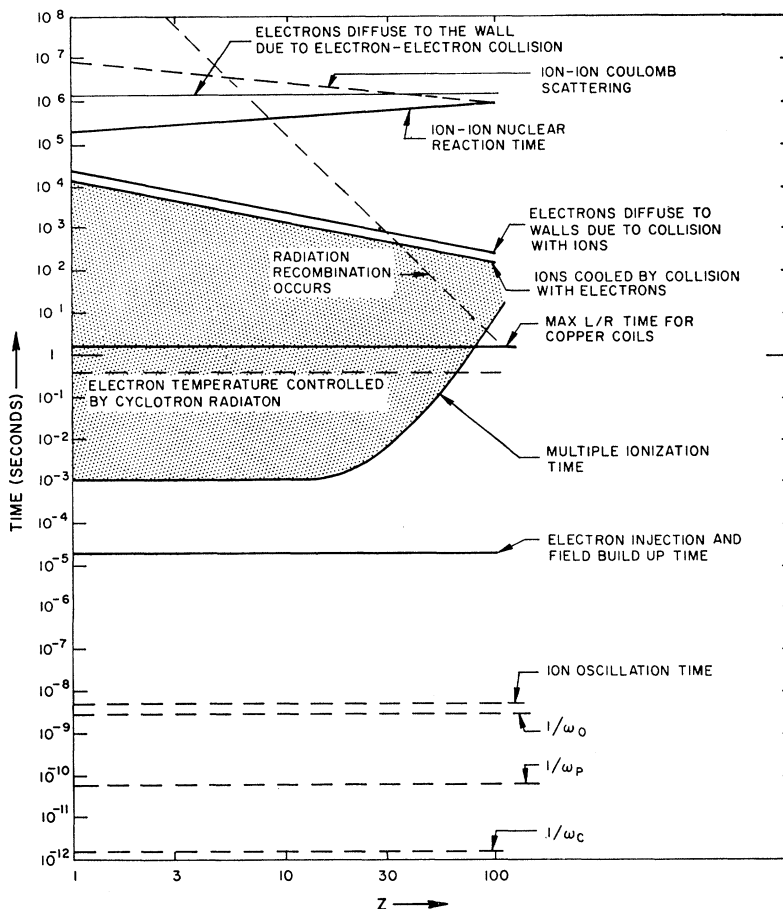
In Fig. 1 we display against  $Z$  the Coulomb nuclear barrier potential and our estimate of the maximum available energy per proton in the center-of-mass coordinate system for the machine described in Table I. It is seen that the maximum available energy for fully stripped atoms is well in excess of the barrier potential for all elements, and that relatively incomplete stripping would be adequate for the lighter elements. Figure 23 displays the minimum degree of ionization which is required for penetration of the Coulomb barrier in a collision between like nuclei in the 20-MeV well depth HIPAC taking into account the effect described in Appendix A. A 20-MeV well depth produces 40 MeV in the center-of-mass coordinate system which, for singly ionized particles, is adequate for penetration of

TABLE II. Yields from proposed Argonne heavy ion cyclotron. (See Ref. 6.) (Assume target of same material as projectile.)<sup>a</sup>

Ion accelerated	Energy (MeV)	Flux (ions/sec)	Effective target thickness (g/cm <sup>2</sup> )	$\mathcal{R}/\sigma$ (reactions/sec cm <sup>2</sup> )
${}^6\text{C}^{3+}$	335	$1 \times 10^{14}$	0.26	$13 \times 10^{35}$
${}^6\text{C}^{4+}$	500	$6 \times 10^{12}$	0.53	$1.6 \times 10^{35}$
${}^7\text{N}^{4+}$	520	$2 \times 10^{13}$	0.38	$32 \times 10^{34}$
${}^7\text{N}^{5+}$	615	$6 \times 10^{11}$	0.52	$1.3 \times 10^{34}$
${}^8\text{O}^{4+}$	450	$1 \times 10^{13}$	0.20	$7.3 \times 10^{34}$
${}^8\text{O}^{5+}$	625	$2 \times 10^{11}$	0.38	$0.29 \times 10^{34}$
${}^{10}\text{Ne}^{4+}$	370	$1 \times 10^{13}$	0.077	$23 \times 10^{33}$
${}^{10}\text{Ne}^{5+}$	560	$2 \times 10^{11}$	0.16	$0.94 \times 10^{33}$
${}^{18}\text{Ar}^{5+}$	285	$1 \times 10^{13}$	0.011	$1.6 \times 10^{33}$
${}^{18}\text{Ar}^{6+}$	420	$3 \times 10^{12}$	0.017	$0.77 \times 10^{33}$
${}^{18}\text{Ar}^{7+}$	560	$2 \times 10^{12}$	0.028	$0.84 \times 10^{33}$
${}^{18}\text{Ar}^{8+}$	720	$4 \times 10^{11}$	0.045	$0.27 \times 10^{33}$

<sup>a</sup> Note: We have assumed a universal energy loss law  $dE/dx = Z_{\text{eff}}^2 f(v)$  with  $f(v)$  the same as for protons and  $Z_{\text{eff}} = Z$ , except for  $\text{Ar}^{6+}$ , for which  $Z_{\text{eff}} = 16$ . We also assume the effective target thickness  $t \approx \frac{1}{2} E / (dE/dx)$  and  $\mathcal{R}/\sigma = \text{flux} \times t \times 6 \times 10^{23} / A$ .

FIG. 24. The principal times relevant to the HIPAC whose parameters are listed in Table I are shown on this figure. The area of useful operation is hatched and is limited on the one hand by the necessity of ionizing at least to the degree indicated in Fig. 23, and on the other by the collisional cooling of the ions. Although nuclear "burn-out" cannot be achieved in this time, a reasonable fraction of the ions can be reacted. The "L/R time" for copper coils corresponds to the natural decay of the magnetic field. The rise in the temperature of the copper accompanying this decay is, however, only a few degrees, so that by supplying power, copper coils could be used for durations comparable with the ion cooling time. Optimization of the duty-cycle based on this type of consideration has not yet been performed. Furthermore, the L/R consideration can be completely eliminated by the use of a superconducting dc field coil as outlined in Appendix C.



the nuclear Coulomb barrier for  $Z < 17$ . Multiple ionization is required for heavier elements, but complete stripping is never required.

In order to establish the operating requirements for this machine, it is obviously necessary to estimate the time required for the production of the required degree of ionization, however, this calculation has been deferred to Sec. III.1. These ionization times must be compared with the characteristic time for oscillation of ions in the potential well. The oscillation time is roughly

$$\tau_{osc} = \frac{1}{\omega_p} \left( \frac{m_p}{m_e} \right)^{1/2} \left( \frac{A}{Z_{eff}} \right)^{1/2} \approx 10^{-9} \left( \frac{A}{Z_{eff}} \right)^{1/2} \text{ sec.} \quad (\text{II.4.29})$$

Comparing  $\tau_{osc}$  with the ionization times estimated in Sec. III.1, it is clear that each ion will cross the system numerous times between ionizations.

It is characteristic of all ion sources that the time for crossing the device in a typical electric field is short compared to the time required to achieve a really high degree of ionization. The great virtue of the HIPAC is that the electric field in the ion source actually traps the ion, and also accelerates it so that all ions will eventually achieve high states of ionization. Ionization, trapping, and acceleration all take place in the same geographical region.

Some of the time scales for various processes in the HIPAC have been calculated; these include the various electron frequencies, (II.4.22), (II.4.23), and (II.4.24), the ion oscillation time (II.4.29), the field buildup time and the nuclear lifetime. These times and others are shown in Fig. 24. The times that have not yet been calculated are derived in the next section. For operation to be reasonable, the HIPAC equilibrium must last longer than the time necessary for adequate ionization (as indicated in Fig. 23) to take place. The most restrictive limit on the duration of the HIPAC is apparently (and assuming stability!) the cooling of the ions as a result of collisions with the electrons. Between the times corresponding to these events is a useful region; the hatched area on Fig. 24 corresponds to this region.

We conclude this section by displaying in graphical summary form the parameters available to the HIPAC when the radius of the cross section  $a$  is chosen as either 10 cm, 20 cm, or 1 m. These graphs, or "maps," are shown in Figs. 25, 6, and 26, and they show how the selection of two parameters (in addition to the size) effectively fixes everything else.

The relations used in calculating these maps were just Poisson's law, the definition of  $q = \omega_p^2 / \omega_e^2$ , and

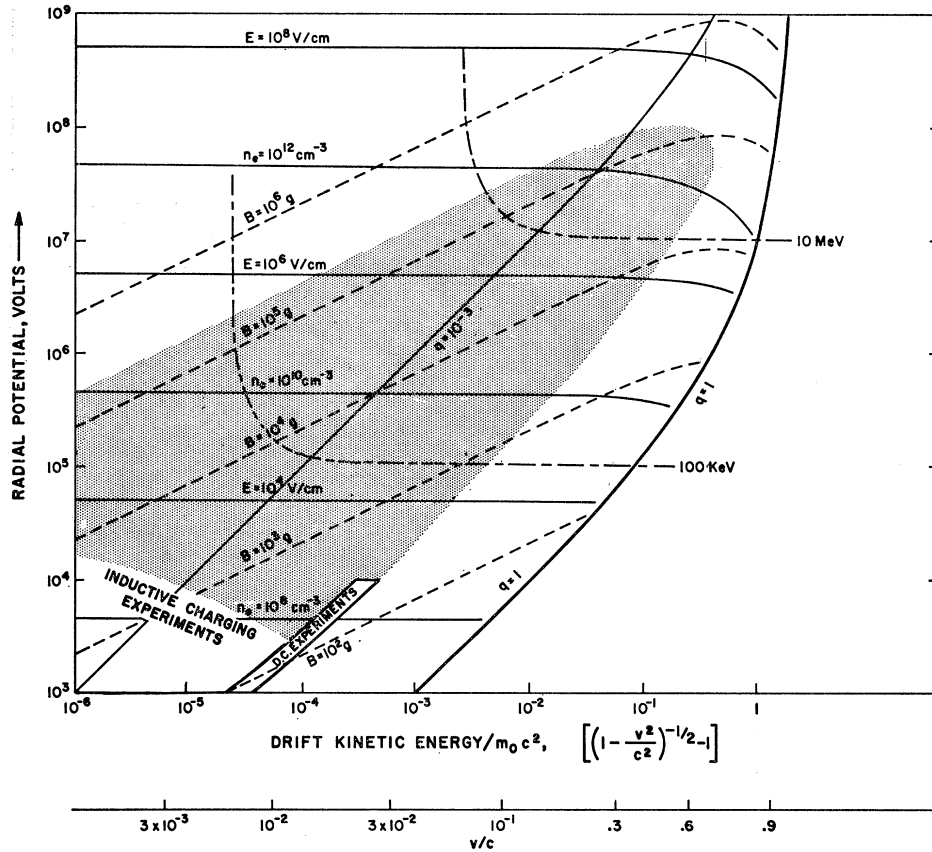


FIG. 25. This “map” shows the various combinations of parameters permissible for a HIPAC having minor radius  $a=10$  cm. The ordinate represents the potential difference between the circular axis and the wall, and the abscissa is  $[(1-v^2/c^2)^{-1/2}-1]$ , where  $v=E/B$ , the drift velocity at the wall. Lines of constant electric field  $E$  (wall value), magnetic field  $B$ , electron density  $n_e$ , and  $q=\omega_p^2/\omega_c^2$  are shown. A proton released at the wall will acquire an energy of 100 keV, or 10 MeV along the lines so marked: the bends in these lines occur roughly where the ion Larmor radius is 10 cm, i.e., the dimension of the HIPAC. For stronger magnetic fields, the proton energy is limited to the value associated with the  $E/B$  drift speed. The hatched area represents an estimate of attainable conditions. It is limited by practically attainable magnetic fields on the order of 100kG, and by the stability boundary at  $q \approx 0.03$ . Experiments already performed are shown in the lower left-hand corner.

$v_{\text{drift}} = E/B$ . Some care was exercised in calculating the effect of the electron current on the applied magnetic field.

The experiments performed so far are picked out on the 10-cm map. The dc experiment is the one illustrated in Figs. 15, 16, and 17, and the inductive charging experiment is the one illustrated in Figs. 11, 12, 13, and 14. It will be seen that a considerable degree of extrapolation is involved in going from the present experiments to a useful HIPAC, but so far there is no indication of any reason why this extrapolation could not be accomplished.

The lines marked 100 keV and 10 MeV (on the 10- and 20-cm maps) and 10 MeV, 100 MeV, and 1 BeV (on the 1-m map) have the following interpretation: They represent conditions under which a proton released at rest at the wall of the HIPAC would acquire the stated energy. Under weak magnetic-field conditions, the requirement is simply that the total potential across the device be the appropriate amount. However, under strong magnetic-field conditions a proton will not penetrate to the region of low potential, and will only acquire an energy corresponding to the  $E/B$  velocity. The bends in these curves occur where the proton Larmor radius equals the apparatus size. Since the proton Larmor radius is nearly 2000 times the electron Larmor radius, and since the ratio of the

electron Larmor radius to the apparatus dimension has been shown to be the ratio  $q$ , it follows that the bends in the curves occur near  $q=1/2000$ . For ions with smaller charge-to-mass ratios the bend would occur at correspondingly smaller values of  $q$ .

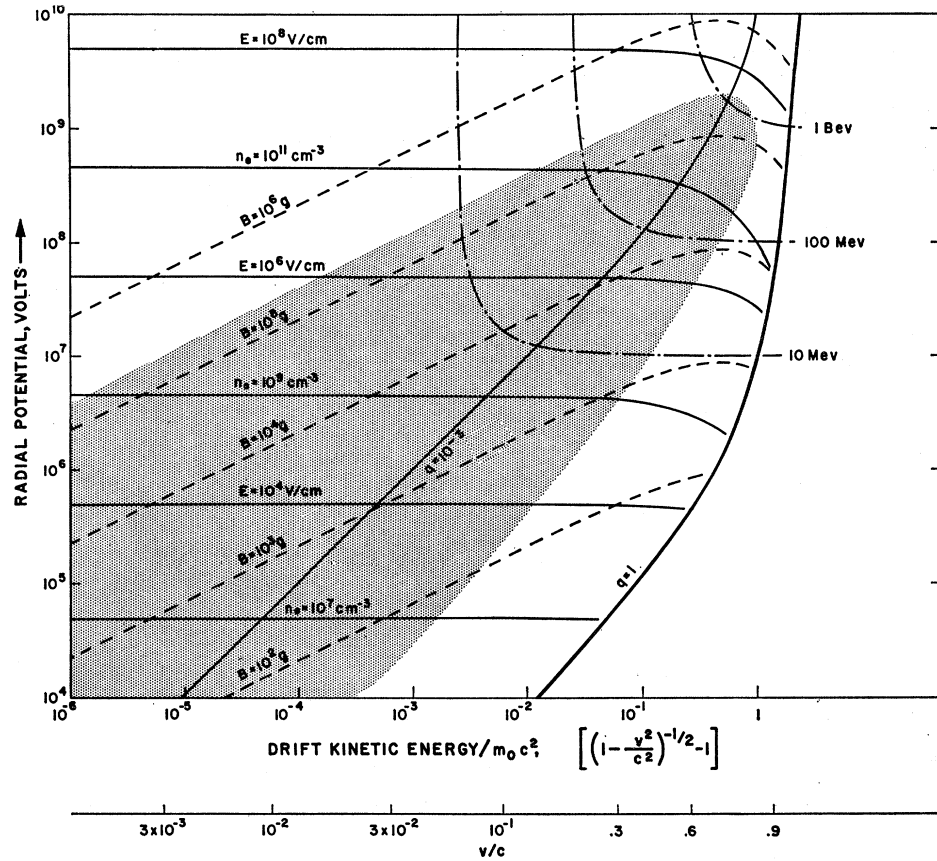
The shaded areas on the maps correspond to an estimate of the range of conditions available to the HIPAC. This area is limited on the one hand by practical magnetic-field strengths ( $\sim 100$  kG) and on the other by a stability boundary in the vicinity of  $q \approx 0.03$ . Note that this boundary has been extrapolated far beyond the range for which there is experimental verification. The extrapolation assumes, for example, that there is no effect of increasing  $v_e/c$  on the location of the boundary.

The HIPAC discussed in detail in this section is represented by the point called “Sample Calculation” on the 20-cm map. For a 20-cm apparatus, this map enables one to estimate other achievable conditions than those listed in Table I.

### III. IONIZATION, COLLISIONS, AND OTHER PROCESSES

We have so far restricted our attention to an idealized stable system in which the ion density is negligible and in which collisional and classical radiative effects have

FIG. 26. This map differs from those shown in Figs. 25 and 6 only in referring to a larger HIPAC—the minor radius is assumed to be 1 m. The lines on this map all have the same significance as their counterparts in Figs. 25 and 6. No experiments have been performed in apparatus as large as this. It can be seen that potentials close to  $10^9$  V may be attainable in apparatus of this size.



been ignored. The applications put forth in this paper require the presence of ions. It is therefore necessary to maintain the electric and magnetic fields for a period of time which is long relative to  $\tau_{ion}$ , the time required to produce the necessary degree of ionization.

In the absence of instabilities, losses due to various classical collisional effects can be expected to control the length of time for which the desired experimental conditions can be maintained. In general, collisional effects will discharge the electric field by allowing electrons to move towards the outside wall and reduce the kinetic energy of the ions. Radiative effects will act as a cooling mechanism which limits the electron temperature.

The possible radiative effects are cyclotron radiation and bremsstrahlung. Collisional-loss effects can arise as a result of electron-ion Coulomb collisions, electron-electron Coulomb collisions, ion-ion Coulomb collisions, charge-exchange collisions, electron neutral collisions, ion neutral collisions, and wall outgassing.

**1. Ionization**

We first proceed to estimate the time required to produce the necessary degrees of ionization for penetration of the Coulomb barrier as estimated in Sec. II-4 and Fig. 23. Ionization can occur by either electron

or ion impact. However, in estimating the time requirements we will primarily concern ourselves with electron impact ionization even though ion impact will contribute quite significantly to the production of multiple ionization in higher Z elements. The resulting time estimates will thus be conservative in that they represent an upper bound to the ionization times.

The cross section,  $\sigma_{j,ion}$ , for removal of the  $j$ th electron from an atom by electron impact is given by Eq. (III.1.1):

$$\sigma_{j,ion} = \frac{K\pi e^4}{[m_e v_e^2/2] I_j} \ln\left(\frac{m_e v_e^2}{2I_j}\right), \quad (III.1.1)$$

where  $I_j$  is the corresponding ionization energy,  $K$  is a constant  $\approx \frac{1}{4}$ ,  $m_e$  and  $e$  refer to the electron mass and charge, respectively, and  $v_e$  is the velocity of the incident electron. In order to find the total cross section,  $\sigma_{ion}$ ,  $\sigma_{j,ion}$  must be summed over all remaining electrons. Since the radiation relaxation times are short relative to ionization times, the inner electrons will be in their lowest energy states which have large values of  $I$ . Thus, the primary contribution to ionization will come from the outer few shells for which  $I$  is relatively small. As the outer electrons are removed, however, contributions from the inner shells will become more and more important.

The value of  $I$  can be estimated by use of Slater's screening constants. In estimating the electron energies and fluxes, we have taken into account both the drift energy and the thermal energy of the electrons. We assume equal thermal and drift energies at injection and include the increase in thermal energy associated with their subsequent adiabatic compression in the rising magnetic field. This leads to an electron-energy distribution which varies as  $r^{-2}$  (i.e., has a maximum at the center) and which has a value of about 18 keV at the outer wall. In estimating ionization rates we have averaged the ion motion over the radial variations in electron flux and electron energy, and taken into account the effects of loss of well depth discussed in Appendix A. The details of these calculations and ionization rates are straightforward but tedious and are therefore not reproduced here. The results are plotted in Fig. 24 which displays the estimated time required to produce the necessary degree of ionization for the attainment of sufficient ion energy to penetrate the Coulomb barrier (see Fig. 1).

2. Radiative Electron Cooling

Before discussing the various collisional diffusion processes, almost all of which contribute to raising the electron temperature, it is important to note that the incoherent cyclotron radiation associated with the electron thermal motion in individual Larmor orbits will contribute to cooling the electrons at a rate such that

$$\frac{d(kT_e)}{dt} = kT_e \left( \frac{B^2}{3} \right) = \frac{kT_e}{\tau_{ce}}, \tag{III.2.1}$$

where  $\tau_{ce} = (3/B^2)$  sec. For  $B = 2.6$  W/m<sup>2</sup>, we have  $\tau_{ce} = 0.45$  sec. This time is long relative to the ionization times for all but the heaviest elements and will not affect the ionization time calculations very significantly. The effects of radiative cyclotron cooling will, however, have to be considered if the plasma is contained for times much longer than a second. Electrons can also radiate energy by virtue of their  $E/B$  circular drift motion; however, the accelerations are much less. In this case, the acceleration of the electron is reduced by the factor  $q$ , and the radiative power by  $q^2$ , while the energy reservoir which is the electric field is increased by  $q^{-1}$ . Times in excess of  $10^6$  sec would be required to radiate away a significant portion of the electric-field energy by this process.

† Bremsstrahlung proceeds at a rate given by Eq. (III.2.2):

$$dP_{\tau}/dt = Z^2 n_i n_e 1.7 \times 10^{-32} (T_e)^{1/2} \text{ W/cm}^3, \tag{III.2.2}$$

or

$$\tau_{Br} = \frac{n_e e T_e}{(dP_{\tau}/dt)} = \frac{T_e^{1/2} 1.6 \times 10^{-19}}{Z^2 n_i 1.7 \times 10^{-32}} = \left( \frac{T_e^{1/2}}{Z} \right) 10^3 \text{ sec.}$$

If  $T_e \approx 10^4$  eV, then

$$\tau_{Br} > \approx 1000 \text{ sec} \gg \tau_{cy}.$$

This is a relatively slow process compared with cyclotron cooling, and can be ignored as a cooling process. Bremsstrahlung also acts to slow down the circumferential electron drift. However, the energy for this process is taken out of the electric field rather than out of the electrons thermal energy. It would require more than  $10^6$  sec to deplete the electric-field energy reservoir by this process.

3. Effects of Electron-Ion Collisions

Electron-ion collisions produce a radial drift of electrons towards the outside wall and also cool the ions.

There are three important particle velocities which must be considered. There are the electron-drift velocity  $E/B$ , the electron thermal velocity  $c_e$ , and the velocity of the ions associated with their motion in the potential well. Because of the nature of the ion acceleration process, the ion velocity can never exceed the electron  $E/B$  drift velocity. Actually, the electron thermal velocity is always comparable with the  $E/B$  drift velocity. Initially, this is a result of the injection and adiabatic compression processes. However, its persistence for times long relative to the cyclotron cooling time is a quantitative consequence of a competition between collisional heating and cyclotron cooling. Discussion of the competition between these processes will be postponed.

Inasmuch as the ions are essentially stationary relative to the electrons, we may use the electron drift velocity  $E/B$  for the purpose of computing the collision rates. In Eq. (III.3.1),  $\tau_{ei}$  is the time required for an electron to undergo a  $90^\circ$  scattering as a result of collisions with ions.

$$\tau_{ei} = \frac{1}{\sigma_{ei}(E/B)n_i}. \tag{III.3.1}$$

In Eq. (III.3.1),

$$\sigma_{ei} = \frac{10^{-13} Z^2}{w_e^2} \text{ cm}^2, \quad n_i = \frac{10^{10}}{Z}, \quad E/B = 7.7 \times 10^9 \text{ cm/sec},$$

and  $w_e = 18 \times 10^3$  eV. Hence,  $\tau_{ei} = 38/Z$  sec. On the average, each  $90^\circ$  collision results in the radial displacement of an electron by a distance  $r_e = (E/B)/\omega_c = qa = 1.7 \times 10^{-3} a$ . Hence, the average time for an electron to move to the outer wall is  $\tau_{a,ei} = \tau_{ei}(a/r_e) = 38/qZ = 220(100/Z)$  sec. Each time an electron moves a distance  $r_e$ , it receives approximately  $(\frac{1}{2}m)(E/B)^2 \approx 18$  keV of energy input to electron temperature from the electrostatic field.

In Eq. (III.3.2) we estimate the mean electron temperature by equilibrating this energy input to the radiative electron cyclotron cooling.

$$kT_e \approx \frac{1}{2} m_e (E/B)^2 \tau_{ce} / \tau_{ei} = 18 \text{ kV} \left( \frac{0.45Z}{38} \right) = \left( \frac{Z}{100} \right) 21 \text{ keV.} \quad (\text{III.3.2})$$

The electrons will also acquire an energy increment of  $m_e(v_i^2/2)$  per  $90^\circ$  collision as a result of the center-of-mass motion of the ions. Since  $v_i$  is smaller than the  $E/B$  velocity ( $[E/B/v_i]^2 \approx 3$ ), we can neglect the effect on electron temperature. This phenomenon does, however, represent a significant ion cooling mechanism. The resulting ion cooling time is estimated in Eq. (III.3.3) and (III.3.4):

$$\frac{d(\frac{1}{2} m_i v_i^2)}{dt} = \frac{N_e}{N_i} \left( \frac{1}{2} m_e v_i^2 \right) \left( \frac{1}{\tau_{ei}} \right) = \frac{1}{2} m_i v_i^2 \frac{1}{\tau_{i \text{ cooling}}}, \quad (\text{III.3.3})$$

where

$$\tau_{i \text{ cooling}} = \tau_{ei} \left( \frac{N_i}{N_e} \right) \left( \frac{m_i}{m_e} \right) = \left( \frac{38}{Z} \right) \left( \frac{1}{10Z} \right) (2Z1837) = \left( \frac{100}{Z} \right) 140 \text{ sec.} \quad (\text{III.3.4})$$

#### 4. Losses Due to Electron-Electron Collisions

Like particle collisions do not represent a diffusion mechanism except in the presence of a gradient in density or temperature. There is no need to maintain electron density gradients significantly steeper than  $(n_e/a)$ . The mean radial diffusion velocity  $\bar{v}$  associated with such a gradient is given by Eq. (III.4.1):

$$\bar{v} = \frac{1}{n_e} \nabla n \left( \frac{r_e^2}{\tau_{ee}} \right) \approx \left( \frac{1}{a} \right) \left( \frac{a^2 q^2}{\tau_{ee}} \right) = \frac{aq^2}{\tau_{ee}}, \quad (\text{III.4.1})$$

where  $\tau_{ee}$  is the mean electron-electron collision time for a  $90^\circ$  deflection ( $\tau_{ee}$  is also the electron-electron thermal equilibration time) and  $q$  is  $(\omega_p/\omega_c)^2 \approx 1.7 \times 10^{-3}$ . The radial electron diffusion time,  $\tau_a$ , associated with this effect is given by Eq. (III.4.2):

$$\tau_{aee} = a/\bar{v} = \tau_{ee}/q^2. \quad (\text{III.4.2})$$

We compute  $\tau_{ee}$  in the usual way using the  $E/B$

velocity for computing the electron temperatures

$$\tau_{ee} = \frac{1}{n_e \sigma E/B} = \frac{1}{1.1 \times 10^{11} \times (7.7 \times 10^9) [10^{-13}/(18 \times 10^3)^2]} = 3.8 \text{ sec.} \quad (\text{III.4.3})$$

Hence,

$$\tau_a = \frac{3.8}{(1.7 \times 10^{-3})^2} \approx 1.3 \times 10^6 \text{ sec.}$$

#### 5. Ion-Ion Coulomb Collisions

Since there are fewer ions than electrons, ion-ion collisions cannot affect the potential distribution. They can, however, affect the ion-velocity distribution. In general, the effect of ion-ion Coulomb collisions will be to transfer some of the ion energy into nonradial components of ion motion and to elevate the energy of some of the ions at the expense of others (i.e., Maxwellize them). In principle, this could result in the ejection of some particle out of the potential well. The mean time for an ion-ion Coulomb scattering which accomplishes either of these effects may be estimated as follows:

$$\tau_{ii} = 1/n_i \sigma v_i,$$

where

$$n_i \approx 10^{10}/Z, \quad \sigma = [Z^4 10^{-13}/(w_i)^2] \text{ cm}^2,$$

and

$$v_i \lesssim 4.5 \times 10^9 \text{ cm/sec.}$$

Since  $w_i = ZV$  and  $V = 2 \times 10^7$  we see that

$$\sigma = Z^2 10^{-13}/V^2 = 2.5 \times 10^{-28} Z^2$$

and

$$\tau_{ii} = \frac{1}{2.5 \times 10^{-28} Z^2 (10^{10}/Z) 4.5 \times 10^9} = \left( \frac{100}{Z} \right) 8.9 \times 10^5 \text{ sec.}$$

Since this is a very long time, the effects of ion-ion collisions can be neglected.

#### 6. Recombination and Charge Exchange Effects

If an ion picks up an electron in the center, near the bottom of the well, and loses it near the top of the well, it will increase its total energy (and vice versa) and a series of such events may eject the ion over the top of the well to the wall. If, however, the particle is in a high state of ionization, the fractional change in its energy per event will be small and a large number of random events will be required before a significant number of ions have acquired enough energy to be ejected in this manner. It is relatively easy for an ion to lose an electron; hence, the rate at which this process

proceeds will depend upon the rate at which electrons can be picked up near the center. The electron (and ion) energies and densities are such that three body recombination is highly unlikely and can be neglected entirely. Radiative recombination is somewhat more probable<sup>40</sup> but still only occurs at a rate of one per second for  $Z=100$  and is much less probable at lower  $Z$  (see Fig. 14).

The most probable way of gaining an electron is by charge-exchange collisions which in themselves do not change the total energy in the ions. Charge-exchange collisions can occur when two atoms approach each other within a distance such that the electron can easily tunnel across from one atom to the other. This distance is proportional to the atomic radii, but somewhat larger. We can thus expect the charge-exchange cross sections to have the same  $(1/Z)^2$  dependence as the cross section for ionization by electrons.

Charge exchange cannot occur if every ion is fully stripped. Our estimated calculations of electron energies indicate that atoms with atomic number  $Z$  in excess of 30 will not be fully stripped by electron-impact ionization. However, ionization by ion impact is always energetically possible and can be expected to proceed at a rate which is almost within a factor of 10 of the rate for charge-exchange collisions, since the ion-impact velocities are almost comparable with the characteristic electron velocities for the residual Bohr orbits. For this reason, we expect that the ions will become fully stripped by ion impact before a sufficient number of charge-exchange collisions have occurred to eject them to the wall.

### 7. Losses Due to Background Gas

It is proposed to fill the HIPAC with electrons to a density of  $10^{11}$   $\text{cm}^{-3}$ . At a background pressure of  $10^{-8}$  mm Hg, the number density of background neutrals would be  $3.5 \times 10^8$   $\text{cm}^{-3}$ . Each neutral will certainly become ionized; and even if each one underwent 28 ionizations (i.e., fully stripped  $\text{N}_2$ ), the depth of the potential well could only be reduced by 10%. This effect can be described as a burnout. While it seems clear that it should occur, it has not yet been observed, since experiments carried out to date have had too short a duration.

### 8. Wall Outgassing

Another source of background gas is outgassing from the walls. Wall outgassing can be described by attributing to the wall an effective vapor pressure which is the minimum pressure which can be obtained in the region near the wall with a perfect pump. If this pressure is  $p_w$ , then in a containment time of  $\tau$  we have an effective background pressure due to wall effects

<sup>40</sup> H. A. Bethe and E. E. Salpeter, *Quantum Mechanics of One- and Two-Electron Atoms* (Academic Press Inc., New York, 1957).

which is equal to  $p_{\text{eff}} = p_w(\tau c^*/a)$  where  $c^*$  is the velocity of sound. Values of  $p_w$  in the range of  $10^{-14}$  mm Hg have been attained and would lead to effective background pressures in the range of  $10^{-8}$  mm for times comparable with 1000 sec. This indicates that a very high quality vacuum system will be required. However, we suspect that the apparatus will tend to clean its own walls by bombardment after being placed in operation.

### 9. Breakdown

At several places in the preceding pages it has been mentioned that it is hoped to generate steady potentials of several tens or even hundreds of millions of volts. Such potentials have not yet been demonstrated and the question arises as to what the effect on the HIPAC will be of the type of breakdown mechanism which limits other types of high-voltage machines. In particular, the highest voltages so far obtained are in the neighborhood of  $10^7$  V, and these are reached in very large and elaborate Van de Graaff machines. Naturally, a definitive answer to this question can only be obtained experimentally.

For the HIPAC, the relevant experience is not so much in the area of the Van de Graaff (in which pressurized dielectrics are commonly employed) as in the area of high vacuum breakdown between plane (or spherical) electrodes. The amount of matter in the HIPAC is quite insufficient to permit any form of gas discharge to occur. There remain only the processes having to do directly with the properties of the electrode surfaces. As we shall see from a review of these processes, it is quite unlikely that the HIPAC can suffer breakdown as the term is currently understood. There are, presently, a number of theories about the origin of electric breakdown in vacuum.<sup>41</sup> These are:

(1) Field emission at the cathode.<sup>42-44</sup> At the negative terminal, electrons are pulled out of the surface by the electric field. The electrons come out by quantum mechanical tunneling of conduction electrons through the potential barrier at the surface of the metal, according to the Fowler-Nordheim theory.<sup>45</sup> On large cathodes most of the current drawn in this way comes from tiny projections on the cathode surface where the electric field is enhanced. Catastrophic breakdown occurs when Ohmic heating of the projection by the field emission current causes the projection to explode.

From the point of view of the HIPAC, there being no material cathode, this mechanism is impossible.

<sup>41</sup> D. Alpert, D. A. Lee, E. M. Lyman, and H. E. Tomaschke, *J. Vacuum Sci. Tech.* **1**, No. 2 (1964).

<sup>42</sup> W. P. Dyke and J. K. Trolan, *Phys. Rev.* **89**, 799 (1953).

<sup>43</sup> W. P. Dyke, J. K. Trolan, E. E. Martin, and J. P. Barbour, *Phys. Rev.* **91**, 1043 (1953).

<sup>44</sup> W. W. Dolan, W. P. Dyke, and J. K. Trolan, *Phys. Rev.* **91**, 1054 (1953).

<sup>45</sup> R. H. Fowler and L. Nordheim, *Proc. Roy. Soc. (London)* **A119**, 173 (1928).

Field emission of ions at the anode by the tunneling process will be negligible at the electric fields contemplated.

(2) Surface regeneration processes. Van Atta *et al.*<sup>46</sup> have proposed as an initiating event for breakdown the interchange of charged atomic particles between cathode and anode, that is, a chain reaction in which particles ejected from one electrode produce particles of the opposite sign upon impact at the other electrode surface. Breakdown occurs when the regeneration coefficient exceeds unity.

This model is clearly not applicable to the HIPAC which has only one electrode.

(3) In the so-called "clump hypothesis," Cranberg<sup>47</sup> has attributed breakdown to the transfer of charged clumps of material ripped from one of the electrode surfaces and accelerated to the opposite electrode. If the particle is given sufficient energy, it will produce upon impact localized temperatures in excess of any known boiling points. Breakdown might then take place in the vapor of the metallic particle if the Townsend criterion for minimum sparking potential is met.

From the point of view of the HIPAC, as it stands, this theory is not applicable. However, it is worth considering the fate of a positively charged "clump" pulled from the wall of the HIPAC by the electric field. Such a clump would immediately be exposed to the crossed-field electron beam and, for reasonable numbers, it is easy to show that the clump would very rapidly be vaporized and ionized. The resulting ions would be trapped in the potential well. There is, therefore, no possibility of a catastrophe caused by impact of the clump with the nonexistent cathode. On the other hand, the trapped ions from even quite a small clump could easily take up the entire energy of the electrostatic field, thereby effectively causing a loss of potential.

It may be guessed that the effect of this phenomenon would be to clean the surface, higher potentials being obtained with clean surfaces.

(4) A theory exists<sup>48,49</sup> which ascribes breakdown as being due to localized heating of the anode caused by narrow beams of electrons drawn by field emission from the cathode. This theory is clearly inapplicable to the HIPAC and need not concern us further.

While we cannot, in this paper, attempt a critical evaluation of these various theories, it is evident that past experience will be a very poor guide in predicting the nature of breakdown in the HIPAC. If it does break down in some identifiable manner, it would be surprising if this did not throw some light on the older

problem, for example by allowing measurements on clumps, if any, drawn from the anode surface, or by clarifying other features of the anode surface.

In summary, existing breakdown theories do not appear to be relevant to the HIPAC. In some ways it might be argued that any serious instability of the electron cloud (Sec. II.3), since it would result in a catastrophic loss of potential, should be regarded as a breakdown initiated from the cathode. Although a plausible case might be made for this extension of the meaning of the word "breakdown," it seems on balance better to reserve the word for its usual meaning (i.e., breakdown between two solid electrodes) and to describe loss of the electron beam due to some coherent oscillation as an instability.

## 10. Summary

The results of the foregoing time calculations have been collected and displayed in Fig. 24 as a function of  $Z$ , the atomic number. The ordinate is time. The estimated available "cooking" time has been hatched. It is bounded on the lower side by the field buildup time and by the time required to produce the requisite degree of ionization. It is bounded on the upper side by electron-ion collision effects which both cool the ions and allow the electrons to diffuse to the walls. The line labeled  $L/R$  corresponds to the time after which the integrated Joule heating in the most efficient copper coil which fits the system exceeds the magnetic-field energy. The primary power requirements are associated with creating and maintaining the magnetic field. Thus, cycle durations longer than a few seconds will inevitably result in an increased energy requirement per nuclear reaction, unless the design involves superconductor or cryogenic coils. Such approaches are believed to be possible, but their economics have not been studied.

In general, the effect of these various forms of loss can be seen to limit the duration of an experiment, but not to limit it to uselessly short times. In this connection it may be noted that the plasma radiation shield<sup>50</sup> (a device closely related to the HIPAC) is expected to decay by diffusion in about 48 h—indeed, it is this long time, which is like the time of duration of a solar flare, which renders the entire concept interesting. For the HIPAC, with its higher densities, smaller sizes and trapped ions, times as long as this cannot be expected. But useful numbers of reactions will occur in times like a second or so, so that larger times than this are quite unnecessary.

## ACKNOWLEDGMENTS

It is a pleasure to acknowledge useful and stimulating discussions held with O. Buneman, J. Callen, H. Haus, A. Kantrowitz, C. Kennel, and H. Petschek.

<sup>46</sup>L. C. Van Atta, R. J. Van De Graaff, and H. A. Barton, *Phys. Rev.* **43**, 158 (1933).

<sup>47</sup>L. Cranberg, *J. Appl. Phys.* **23**, 518 (1952).

<sup>48</sup>W. H. Bennett, *Phys. Rev.* **45**, 890 (1934).

<sup>49</sup>W. S. Boyle, P. Kisliuk, and L. H. Germer, *J. Appl. Phys.* **26**, 720 (1955).

<sup>50</sup>R. H. Levy and G. S. Janes, *AIAA J.* **2**, 1835 (1964).

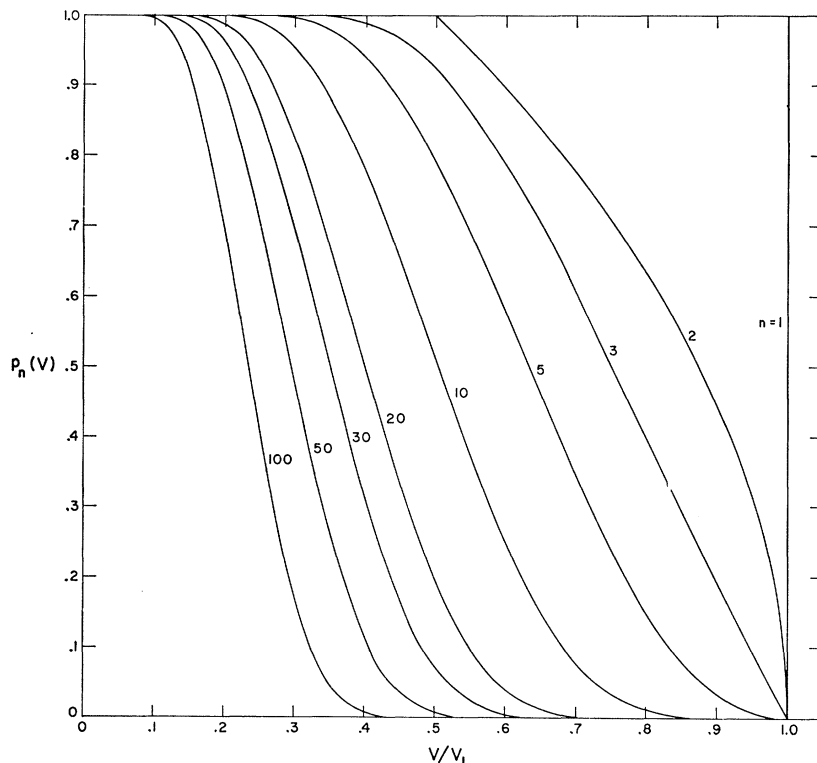


FIG. 27. A singly ionized particle is released at rest at potential  $V_1$ . After  $n$  ionizations it has a well depth  $V_n \leq V_1$ . This graph shows  $p_n(V)$ , the probability that  $V_n \geq V$ . The expected (mean) value of  $V_n$ , and the variance are shown in Fig. 22. The assumptions and method of calculation used are discussed in Appendix A.

#### APPENDIX A: LOSS OF WELL DEPTH IN MULTIPLE IONIZATION

Ideally, every ionization in the HIPAC would take place very near the wall; this is because such ionizations increase the ion energy as much as possible. In practice, however, ionizations may take place at a distance from the wall; following such ionizations the particles cannot regain their previous minimum distance from the wall, and, when passing the bottom of the potential well, will have less than the ideal energy. We seek a quantitative (probabilistic) description of the effects of this phenomenon on the distribution of ion energies after up to about 100 ionizations.

The probability of ionization per volt of potential crossed by an ion is  $\sigma n_e v_e / v_i E$ ; the symbols are the appropriate cross section, the electron density and velocity, the ion velocity, and the electric field. We have assumed  $v_i \ll v_e$ . For the electron velocity we use the thermal velocity produced by the magnetic compression process. This yields  $v_e^2 \propto B$  at injection, or  $v_e^2 \propto r^{-2}$  spatially. Neglecting a logarithmic factor, we assume  $\sigma \propto v_e^{-2} \propto r^2$ . If we further assume  $n_e$  constant, then  $E \propto r$  and  $\sigma n_e v_e / E$  is approximately constant. It follows that the probability of ionization per volt varies as  $v_i^{-1}$ , which is the factor expressing the fact that the ion spends most of its life at low velocity and high potential.

We further assume that the probability of any ionization taking place on a single pass across the HIPAC is small. With this assumption we can evaluate the

probability  $p_n(V)$ , that after  $n$  ionizations the ion is oscillating in a well of depth  $V_n \geq V$ .  $p_n(V)$  is also the probability that the ion energy at this stage is greater than  $neV$ . The detailed evaluation is given elsewhere,<sup>51</sup> and yields the result:

$$p_n(V) = \int_0^1 p_{n-1} \left( \frac{V}{1-x^2/n} \right) dx. \quad (\text{A1})$$

On the assumption that  $p_1(V) = 1 (V < V_1)$  and  $= 0 (V > V_1)$ ,  $p_n(V)$  is plotted in Fig. 27 for  $n$  up to 100. The expectation  $\mathcal{E}(V_n) = \mathcal{E}_n$  can be expressed directly as

$$\mathcal{E}_n = \frac{\Gamma(n + \frac{2}{3})}{\Gamma(n+1)\Gamma(5/3)} V_1 \sim \frac{1.1}{n^{1/3}} V_1, \quad (\text{A2})$$

the last expression being an asymptotic approximation. A similar result can be obtained for the standard deviation  $\sigma_n$ . Both  $\mathcal{E}_n$  and  $\sigma_n$  are shown in Fig. 22. It appears that for  $10 \leq n \leq 100$  most particles will have well depths on the order of  $\frac{1}{3}$  of their original well depth. Similar calculations with other assumptions regarding the radial distribution of electron temperature and density yield exponents of  $n$  which are not too different from the value  $\frac{1}{3}$  given in Eq. (A2).

<sup>51</sup> G. S. Janes, R. H. Levy, H. A. Bethe, and B. T. Feld, Avco-Everett Research Laboratory Research Report 235, 1965 (unpublished).

### APPENDIX B: NUCLEAR DIAGNOSTICS

The HIPAC is a machine of the "clashing-beam" type rather than a machine producing a highly collimated beam of monoenergetic ions. It is worth making the point that the reason for going to a machine of this type is somewhat different from the reason for considering clashing beams as a useful tool for high-energy physics. In the case of high-energy physics, the basic reason is to overcome the relativistic loss of center-of-mass energy. In our case, we are not dealing with appreciably relativistic particles: rather, the reason for considering a clashing-beam device is that it enables one to make a *closed* trapping region (potential well) in which there are no solid surfaces, and in which the containment time is long enough to accomplish complete stripping. Of course, as a clashing-beam machine, the diagnostics and other experimental arrangements will be substantially different from collimated beam arrangements.

The experimental problem of extracting the information on nuclear reactions produced in the HIPAC will present new problems requiring serious study. It has only been considered in a most preliminary fashion at this stage. The most direct application is one in which the ions introduced as a gas into the accelerator serve as both projectile and target. The reaction products are produced in this gas, but would eventually be deposited on the walls unless special extraction procedures are introduced. Probably the simplest such would involve establishing a region (protrusion) of low potential on the wall of the accelerator, on which there would be a tendency for ions to be deposited. This "catcher" would be removed at an appropriate time, the various reaction products extracted by appropriate radiochemical techniques and their radiations and other properties studied.

The frequency of removal of the "catcher" and performance of the chemical extraction of reaction products, would, of course, depend on the mean life of the radioactivity in question. For lifetimes shorter than, or on the order of, the cycle time of the HIPAC, extraction would have to be performed after each pulse. For longer lived nuclei, the products of many pulses could be accumulated.

In some special cases, it might be possible to extract reaction products as a gas, possibly using mass-spectrometer techniques to separate and identify different radioactive species without the necessity of resort to chemistry. This possibility, especially if the gas extraction could be continuous, would be most significant for the study of very short-lived radioactive species.

Some preliminary consideration has been given to the possibility of utilizing a solid target. Such a target could be provided by inserting into (or dropping through) the device a pellet of the target material in such a way that it would be at the center of the device at the time of maximum voltage. The reaction products

produced in this target could then be extracted by conventional techniques after the pellet emerged from the device. However, simple computations indicate that the energy accumulated by the target during its passage would be sufficient to evaporate a surface layer in excess of the range of the projectile nuclei; hence, the reaction products would remain in the device, to be extracted by other means, such as discussed in the preceding. Nevertheless, such introduction of targets of foreign material might still be highly desirable as a means of increasing the range of reactants available.

### APPENDIX C: A SCHEME FOR GENERATING FAST-RISING LONG-DURATION MAGNETIC FIELDS

There are several possible methods of producing a magnetic field with both a short rise time and a long steady-state time duration. One of the simplest systems consists of a dc field coil (which may be superconducting) inside of which is located an ac coil which is pulsed for one-half of a cycle in order to temporarily reduce the dc field to zero for a short period of time. Such an arrangement is indicated schematically in Fig. 28. The resulting magnetic field history is indicated in Fig. 29.

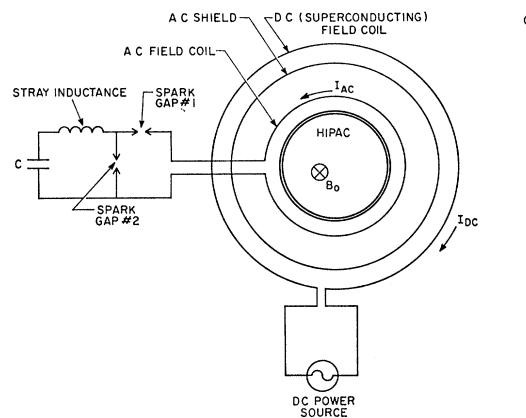


FIG. 28. Schematic diagram of possible apparatus for use in generating fast-rising long-duration magnetic fields in the HIPAC.

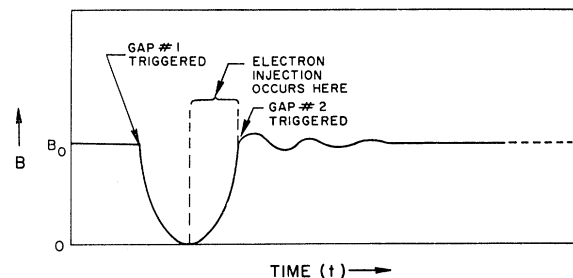


FIG. 29. Time history of the magnetic field in the HIPAC produced by the arrangement shown in Fig. 28.

The sequence of operations is as follows. First the dc magnetic field  $B_0$  is produced at relatively slow pace by building up the current in the dc superconducting field coil from an external power source. The capacitor  $C$  is then discharged through gap No. 1 causing the magnetic field in the HIPAC to temporarily decrease to zero as a result of currents flowing in the external ac field coil. The electron injection occurs on the second

half of the ac cycle while the ac current is returning to zero and the magnetic field is returning to  $B_0$ . When the ac current has returned to zero, the capacitor  $C$  is charged in the reverse direction. At this point, spark gap No. 2 is ignited, short circuiting the ac coil and quenching the current in spark gap No. 1. The function of the ac shield is to prevent image currents from heating the dc superconducting field coil.

## Effect of Backscattering on the Helicity of $\beta$ Radiation

L. BRAICOVICH,\* B. DE MICHELIS, AND A. FASANA

*Istituto di Fisica del Politecnico, Milano, Italy*

(Received 20 December 1965)

Experimental investigation has been carried out on the dependence on the energy of the average longitudinal polarization of  $\beta$  particles of  $^{90}\text{Sr}+^{90}\text{Y}$ , backscattered by a lead target. The ratio of the polarization of backscattered to incident electrons was obtained in the energy ranges 0.3–0.8, 0.55–1.2, and 0.75–2.0 MeV with respective results of  $0.657 \pm 0.192$ ,  $0.503 \pm 0.284$ ,  $0.650 \pm 0.369$ . The effect of a perturbing magnetic field on helicity was also studied. The results are discussed with reference to the mechanism of the backscattering process.

### 1. INTRODUCTION

THE main features of the  $\beta$ -radiation longitudinal depolarization were experimentally investigated by transmitting electrons through foils of different materials<sup>1,2</sup>; on the other hand the depolarization of electrons due to backscattering has not yet been carefully investigated. This paper describes our research on the effect of backscattering from lead on helicity of the  $\beta$  radiation from a  $^{90}\text{Sr}+^{90}\text{Y}$  source; the average polarization of the backscattered electrons was meas-

ured by a Møller polarimeter at different energy intervals.

The effect on the depolarization of a static magnetic field perpendicular to the backscatterer was also investigated with the aim of further clarifying the mechanism of depolarization in the backscattering process.

### 2. EXPERIMENTAL METHOD

#### A. The Apparatus

The Møller-type polarimeter, used in our measurements, was the same as described in one of our previous papers.<sup>2</sup> The collimators were enlarged in such a way that the electrons entering the polarimeter were received in a solid angle of about  $1.4 \times 10^{-3}$  sr, and the electrons scattered by the analyzer foil in the angular range between  $26^\circ$  and  $48^\circ$  were detected.

Three sources of  $\beta$  radiation were employed: each source consisted of 50 mCi of  $^{90}\text{Sr}$  ( $E_{\text{max}}=0.545$  MeV), evaporated into a sintered alumina holder, covered by a layer of stainless steel 0.1 mm thick; the diameter of the active area was 10 mm. The  $^{90}\text{Sr}$  is in equilibrium with its daughter  $^{90}\text{Y}$  ( $E_{\text{max}}=2.26$  MeV). The depolarizer target was a disk of lead, of a thickness equal to the range of the  $\beta$  rays of  $^{90}\text{Y}$ . The target was placed on the surface of the magnet pole, as may be seen in Fig. 1. The magnetic-induction value was 1740 G at the position of the target; the variation of the magnetic field was about 3 and 5% along the thickness and along the radius of the backscatterer, respectively.

The three sources were located at  $60^\circ$  from each other on a plane parallel to the target.

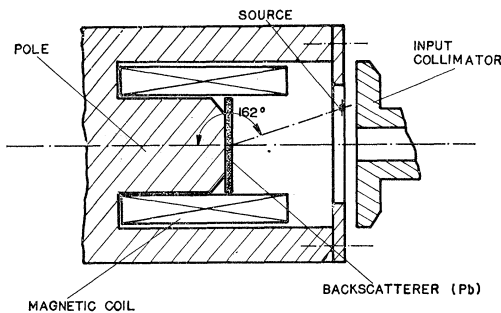


FIG. 1. Geometrical arrangement of the source, the backscatterer, and the input collimator of the polarimeter; the magnetic circuit is also shown.

\*Istituto di Fisica del Politecnico di Milano and Gruppo Nazionale di Struttura della Materia del Consiglio Nazionale delle Ricerche.

<sup>1</sup>J. Van Kinklen, K. Bulthuis, and R. J. Van Duinen, Nucl. Phys. 61, 593 (1965).

<sup>2</sup>L. Braicovich, B. De Michelis, and A. Fasana, Nucl. Phys. 63, 548 (1965).

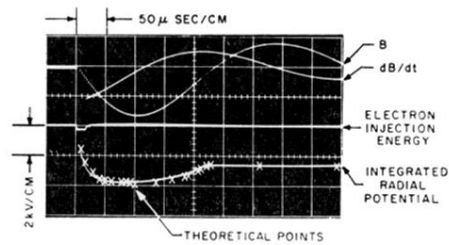


FIG. 12. A typical oscillogram obtained with the apparatus illustrated in Fig. 11. In the upper half, the traces show  $B$  and  $\dot{B}$ ; the quarter-cycle time was  $100 \mu\text{sec}$ . The trace near the axis shows the voltage applied to the electron gun; this was about  $200 \text{ V}$  for  $15 \mu\text{sec}$ . The lowest trace shows the variation of the potential between the inner and outer cylinders. A maximum of  $4 \text{ kV}$  was achieved, representing a voltage multiplication ratio of 20. More importantly, the distribution of electrons at different times was calculated assuming ideal adiabatic motion. At each instant of time, the distribution was integrated to give the radial potential; account was taken of the collection by the inner cylinder of electrons whose field lines were compressed inside it. These calculations are indicated by crosses, and are in excellent agreement with the experimental data. The residual potential at the end of the experiment represents the electrons collected by the inner cylinder.

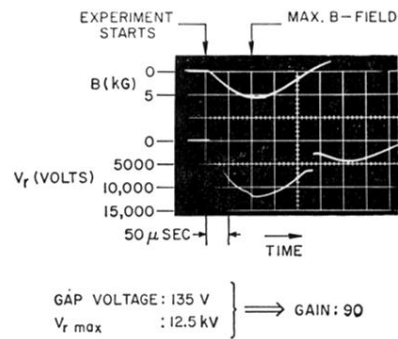


FIG. 14. Results obtained with the apparatus of Fig. 13. The upper trace is  $B$ ; it peaks at about  $100 \mu\text{sec}$ . The lower trace is the potential between the cylinders. The maximum gap voltage (induced by  $B$ ) was 135 V, the peak voltage between the cylinders was 12.5 kV, yielding a gain of about 90. The traces have no significant interpretation after the magnetic field declines to zero due to the occurrence of discharge on the insulating end plates. A simple estimate of the injection current and hence voltage history that this arrangement should yield has been made. The measured voltage history is in good agreement with this prediction.